 doi: 10.1111/j.1365-246X.2005.02657.x

Three-dimensional V_P and V_S structural models associated with the active subduction and collision tectonics in the Taiwan region

Kwang-Hee Kim,[1,2,3] Jer-Ming Chiu,[1] Jose Pujol,[5] Kou-Cheng Chen,[3] Bor-Shouh Huang,[3] Yih-Hsiung Yeh[3] and Peng Shen[1,4]

[1] *Center for Earthquake Research and Information, The University of Memphis, Memphis,* TN 38152, *USA. E-mail: jerchiu@memphis.edu*
[2] *Institute of Geophysics, National Central University, Chung-Li, Taiwan*
[3] *Institute of Earth Sciences, Academia Sinica, Nankang, Taipei, Taiwan*
[4] *Department of Earth Sciences, Rice University, Houston, Texas, USA*
[5] *Department of Earth Sciences, The University of Memphis, Memphis,* TN 38152, *USA*

Accepted 2005 April 11. Received 2005 April 8; in original form 2004 September 15

SUMMARY

3-D V_P and V_S models for the crust and upper mantle beneath the Taiwan area have been determined using selected high-resolution earthquake data from an island-wide seismic network and two local seismic arrays. Lateral structural variations in the upper crust, as also evident from surface geology, are responsible for the observed large traveltime residuals or station corrections. Prior shallow velocity information inferred from traveltime residuals and joint hypocentral determination (JHD) station corrections for the uppermost crust is essential to facilitate a reliable tomographic inversion. A finite-difference method, that is efficient and accurate for a highly heterogeneous velocity structure, is applied to calculate *P*- and *S*-wave traveltimes from the source to receiving stations. All earthquakes in the Taiwan Central Weather Bureau's catalogue are then relocated using the resultant 3-D V_P and V_S models. The depth of the Moho varies significantly, especially along the east–west direction. In the western Coastal Plain and Western Foothills the depth of the Moho is around 35 km, which deepens gradually eastward, reaches a maximum depth of ∼55 km beneath the eastern Central Mountain Range, shallows up rapidly beneath the Longitudinal Valley and Coastal Range, and merges with the thin Philippine Sea Plate offshore of eastern Taiwan. In central Taiwan, the Central Mountain Range is bounded to the east and west by two steeply westward dipping active faults from the upper crust to a depth of about 30 km. Therefore, the uplifted and thickened Central Mountain Range serves as a backstop for the converging Eurasian and Philippine Sea plates. The crust beneath the Central Mountain Range is characterized by a brittle, high-velocity and seismically active upper crust ($<$15 km) and a ductile, low-velocity and aseismic mid-to-lower crust (below 15 km), most probably due to the high geothermal activity from the excess heat supplied from the hot upper mantle beneath the thin oceanic crust to the east, from the surrounding hotter upper mantle beneath the thickened continental crust, and from shear heating during active collision. The collision zone in eastern Taiwan is characterized by an active and steeply eastward dipping seismic zone along a region of low V_P and high V_P/V_S ratio near the Taitung region in southeastern Taiwan. It transforms into an active westward steeply dipping seismic zone along a transition zone between the high V_P and V_S oceanic crust and the low V_P and V_S continental crust near Hualien region in central eastern Taiwan. There is no apparent seismicity within many sedimentary basins imaged from the tomographic inversion. However, a few basins are either bounded on one side by an active fault or are characterized by blind faults beneath. The geometry of the subduction zone in northeastern Taiwan can be clearly imaged from the relocated earthquake locations. Behind the subduction, a region of low V_P and high V_P/V_S ratio at depths of 5 to 10 km can be identified beneath the Tatun-Chilung volcano group indicating a potential magma reservoir. Two steeply dipping linear seismic zones in the volcano region may mark the upward escape paths of the magmatic materials in the region.

Key words: plate collision, subduction, 3D Tomography.

INTRODUCTION

The active and young tectonics and the associated high seismicity in Taiwan provide us with a unique natural laboratory for exploring and understanding the properties of Earth processes in the region. The vigorous processes of mountain building, plate subduction, collision between plates and frequent large earthquakes in the Taiwan region have long been the focus of research for Earth scientists. Since the beginning of the modernization programme of the seismic network instrumentation in 1991, abundant high-quality and high-resolution seismological data have been collected by the island-wide seismic network and a few localized temporary seismic array experiments. The recently available high-resolution earthquake and other geophysical data were explored by many studies with the aim of developing various models to explain the tectonic processes in the Taiwan region (e.g. Rau & Wu 1995; Ma *et al.* 1996; Yen *et al.* 1998). Rau & Wu (1995) used selected data from the Central Weather Bureau (CWB) seismic network to image the lithospheric structure beneath Taiwan and found a very significant variation of crustal thickness across the entire island. Ma *et al.* (1996) used selected data from a similar CWB database and suggested that the estimated crustal thickness beneath Taiwan varies between 30 and 35 km. Based on gravity modelling along a few selected east–west profiles, Yen *et al.* (1998) reported that crustal thickness beneath the Central Mountain Range is ∼33 km. They have also reported that the lack of correlation between the observed Bouguer gravity anomaly and local topography may suggest that isostatic stability of the Taiwan region may not yet have been achieved. Based on magnetotelluric observations, Chen *et al.* (1998) proposed that the depth of the Moho discontinuity is 20 to 30 km beneath the Central Mountain Range. From the modelling and interpretation of seismic data of a wide-angle east–west airgun profile across the southern cross-island highway, Yeh *et al.* (1998) suggested that the crustal thickness of the Philippine Sea Plate under the Pacific Ocean is about 10 km. It thickens rapidly to 50 km beneath the Central Mountain Range. Further to the west of the Central Mountain Range it becomes about 36 km below the Coastal Plain and Western Foothills. From the other wide-angle seismic profile along the central cross-island highway, Shih *et al.* (1998) showed slightly different images of crustal structure, especially for the lower crust, from that of the southern profile (Yeh *et al.* 1998). From these studies, it is evident that the Moho configuration beneath the Taiwan region has not been consistently imaged. Thus it is essential not only to determine a reliable high-resolution crust and upper-mantle structure beneath the Taiwan region but also to validate the resultant structure model using other independent methods.

In this study, representative 3-D V_P and V_S models for the crust and upper mantle beneath Taiwan are determined from a 3-D tomographic inversion using abundant high-quality and high-resolution earthquake data collected by an island-wide seismic network and by two temporary seismic arrays. The inversion program deployed in this study is capable of dealing with traveltime calculation across a highly heterogeneous structure (Podvin & Lecomte 1991; Benz *et al.* 1996), which is the case for the Taiwan region. In order to validate the resultant 3-D velocity structural models for the Taiwan region, a checkerboard resolution test and a restoring resolution test (Zhao *et al.* 1992; Hole *et al.* 2000) have been applied to explore the spatial resolution of critical subsurface structural features from the existing configuration between the stations and background seismicity. Furthermore, Pujol (1995, 2000) demonstrated that a critical criterion to validate the resultant 3-D velocity model obtained from a 3-D tomographic inversion is that the synthetic joint hypocentral determination (JHD) station corrections generated from the resultant 3-D models must be consistent with those from the observed data. After the 3-D V_P and V_S models were validated, they were used to relocate all the earthquakes in the CWB catalogue using a recently developed location algorithm (Chiu *et al.* 2003; Chen *et al.* 2005). Thus, reliable 3-D velocity models and a well-located background seismicity using these models provide an unprecedented opportunity to explore essential structural and tectonic features beneath the Taiwan region.

TECTONIC BACKGROUND

One of the most active tectonic processes on Earth can be observed near the island of Taiwan where the Eurasian Plate and the Philippine Sea Plate are converging (Fig. 1). The Taiwan orogeny is relatively young in the geological timescale. Evidence from the study of sedimentation rate and palaeomagnetism reveals that the mountain building process in the Taiwan region started about 4 Ma (Suppe 1984). A high rate of crustal deformation has been reported by modern levelling and GPS observations (Yu & Liu 1989; Liu *et al.* 1990; Yu *et al.* 1997; Angelier *et al.* 1997). Earthquakes in Taiwan are a consequence of the active tectonic processes related to the collision and subduction of plates (Wang *et al.* 1994). The most prominent seismic features in Taiwan and its surrounding regions can be closely related to a collision system between two active subduction systems, the subducting Philippine Sea Plate beneath the Eurasian Plate in northeastern Taiwan and the subducting South-China Sea Subplate beneath the Philippine Sea Plate in southern Taiwan. The two subduction systems have been recognized since the availability of modern instrumental earthquake data in the early 1970s (Tsai 1986). The Longitudinal Valley is the surface expression, or the suture zone, of the collision system and is characterized by its NNE–SSW trending linear seismicity and topographic features.

Taiwan can be subdivided into two major tectonic provinces separated by the Longitudinal Valley. The eastern province consists of the Coastal Range and a few small islands. The Coastal Range is a remnant of a Neogene island arc, which is the leading edge of the Philippine Sea Plate. The western province can be subdivided into a few distinct NNE–SSW trending structural belts based on petrology. These tectonic units from west to east consist of the Coastal Plain, the Western Foothills, the Hsueshan Range and the Central Mountain Range. These units are often separated or bounded by faults or other structural discontinuities. Each unit has undergone different degrees of metamorphism. It is generally observed in the western province that the closer the region is to the suture zone (the Longitudinal Valley), the higher the grade of metamorphism. The Western Province in western Taiwan is associated with the Eurasian continental shelf (Ho 1999) where crustal seismicity is widely distributed among various tectonic units. However, a large portion of the region beneath the Central Mountain Range has been 'aseismic' since the beginning of modern seismic monitoring in early 1970s and prior to the 1999 Chi-Chi earthquake. A large area of this previously aseismic region became seismically active during and after the 1999 Chi-Chi earthquake.

A few sedimentary basins along western Taiwan are readily observed from the topography and surface geology. Thick sediments in these basins may contribute to the observed low Bouguer gravity anomalies (Yen *et al.* 1998) as well as very significant positive traveltime delays for both *P* and *S* waves. However, a relatively high Bouguer anomaly is observed in the Peikang region of western Taiwan, which can be associated with the Peikang basement high

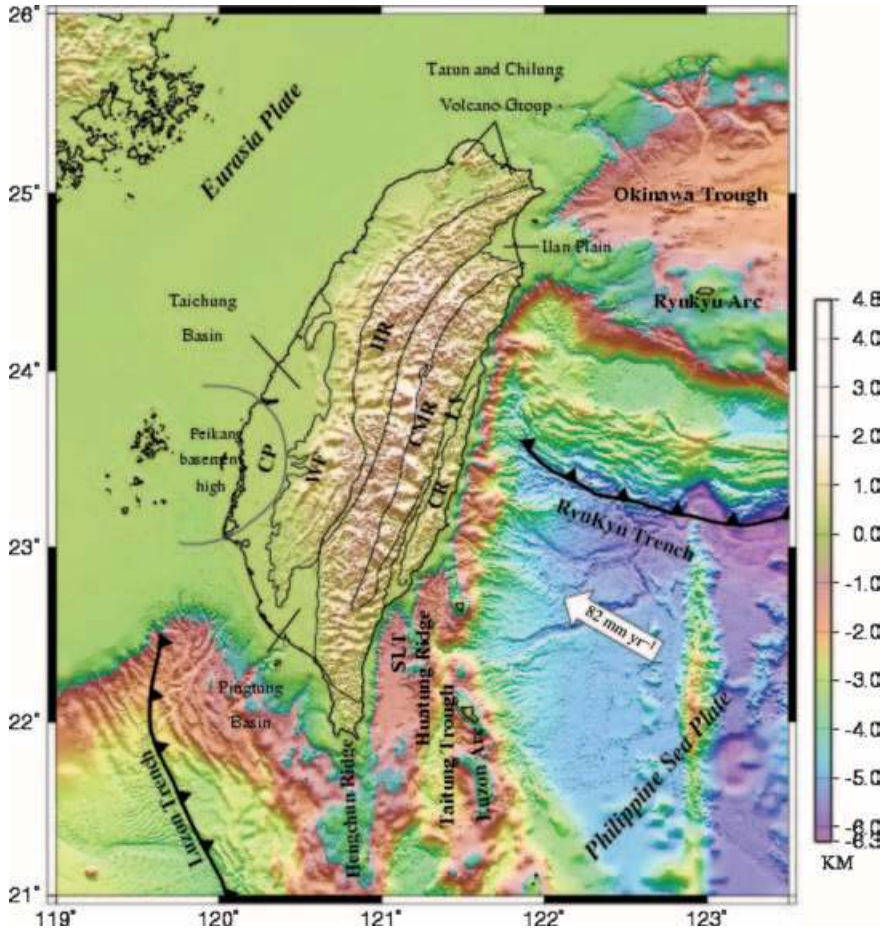

Figure 1. Topography, bathymetry and tectonic setting of Taiwan and its surrounding area. The Philippine Sea Plate is converging towards the Eurasian Plate at a rate of 82 mm yr^{-1} (Yu *et al.* 1997). General geological divisions in Taiwan are presented on top of the topography map (after Ho, 1999), including: CP, Coastal Plain; WF, Western Foothills; HR, Hsueshan Range; CMR, Central Mountain Range; LV, Longitudinal Valley; CR, Coastal Range; SLT, southern Longitudinal Valley Trough.

that is believed to serve an important role as a rigid backstop in the Taiwan orogenic process (Hu *et al.* 1997; Wang & Shin 1998).

METHODOLOGY

The tomographic inversion and relocation package developed by Benz *et al.* (1996) and modified by Shen (1999) was used. This software package includes the ray tracing software of Podvin & Lecomte (1991), which was designed to handle large lateral velocity variations. Benz's software has been successfully applied to data from complex geological settings (e.g. Benz *et al.* 1996; Okubo *et al.* 1997; Villasenor *et al.* 1998; Shen 1999). The inversion and relocation algorithm has been described elsewhere (Benz *et al.* 1996; Shen 1999; Kim 2003); here we will highlight the main results. The velocity model is parametrized in terms of constant-velocity blocks of constant size. Because of the mathematical simplification it introduces, slowness (reciprocal of velocity) is used as an inversion parameter. The process is iterative, and for each earthquake, indicated with the subindex i, we have the following vector equation:

$$\mathbf{r}_i = \mathbf{A}_i \Delta h_i + \mathbf{B}_i \Delta u. \tag{1}$$

where $\mathbf{r}_i$ is the vector of arrival time residuals, $\mathbf{A}_i$ is the matrix of partial derivatives of time with respect to the hypocentre parameters and origin time, Δh_i is the vector of adjustments to the source parameters, $\mathbf{B}_i$ is a matrix that contains the lengths of the ray paths in each of the blocks for each source–station pair and Δu is the vector of slowness adjustments. To decouple the source and slowness unknowns in eq. (1) the method of separation of parameters (Pavlis & Booker 1980) is used, which leads to

$$\mathbf{r}'_i = \mathbf{B}'_i \Delta u. \tag{2}$$

where the primed variables are obtained by multiplication of the corresponding unprimed variables by an appropriate matrix derived from the singular value decomposition (SVD) of the matrix $\mathbf{A}_i$. All of the vector eq. (2) are coupled through the common vector Δu and can be written in a single equation

$$\mathbf{B}' \Delta u = \mathbf{r}' \tag{3}$$

where $\mathbf{B}'$ and $\mathbf{r}'$ are obtained by concatenation of all the $\mathbf{B}'_i$ and $\mathbf{r}'_i$, respectively. To minimize solution instability the model roughness or the degree of variation in slowness, the requirement that the Laplacian of the slowness field vanish is introduced (Lees & Crosson 1989). The resulting system of equations can be written as

$$\begin{bmatrix} \mathbf{B}' \\ sE \end{bmatrix} \Delta u = \begin{bmatrix} \mathbf{r}' \\ 0 \end{bmatrix}, \tag{4}$$

where E is the set of smoothness-constraint equations and s is a smoothing parameter which defines the trade-off between the minimization of the data misfit and model roughness. Decreasing the

value of the smoothing parameters will increase the oscillations in the elements of the Δu, and thus in the final velocity model. System (4) is sparse and is solved using the LSQR algorithm (Paige & Saunders 1982). To relocate the events Benz *et al.* (1996) assumed constant V_P/V_S, but here we used the independently determined *P*- and *S*-wave 3-D velocity models and the following formulation (Pujol *et al.* 1989; Shen 1999). From eq. (1) we have

$$\begin{aligned} \mathbf{r}_i^P &= \mathbf{A}_i^P \Delta h_i + \mathbf{B}_i^P \Delta u^P \\ \mathbf{r}_i^S &= \mathbf{A}_i^S \Delta h_i + \mathbf{B}_i^S \Delta u^S, \end{aligned} \tag{5}$$

where superscripts ^{P} and ^{S} indicate *P* and *S* wave, respectively. The two eqs (5) show that they are coupled through Δh_i, which is the only unknown. After rearranging terms, these equations become

$$\begin{bmatrix} \mathbf{A}_i^P \\ \mathbf{A}_i^S \end{bmatrix} \Delta h_i = \begin{bmatrix} \mathbf{r}_i^P - \mathbf{B}_i^P \Delta u^P \\ \mathbf{r}_i^S - \mathbf{B}_i^S \Delta u^S \end{bmatrix}. \tag{6}$$

Eq. (6) is solved using the singular value decomposition. After updating the hypocentre parameters a new iteration is started.

The number of earthquakes selected for the joint velocity inversion and relocation reported here is less than 5 per cent of the total number of events in the CWB catalogue. However, for a reliable tectonic interpretation all locatable earthquakes in the CWB catalogue should be relocated using the 3-D V_P and V_S models determined by inversion, which was done using the newly developed single-event location algorithm of Chiu *et al.* (2003) and Chen *et al.* (2005).

DATA AND ANALYSIS

Arrival time data

Three sets of high-quality earthquake data recorded by a large number of permanent and temporary seismic stations in Taiwan are used for the seismic tomography and seismicity study. They are earthquake data recorded by the island-wide Taiwan Seismic Network (TSN), the Portable Array for Numerical Data Acquisition II (PANDA II), in the Hualien area of eastern central Taiwan, and the Portable Array for Numerical Data Acquisition (PANDA), in the Pingtung region of southern Taiwan (Fig. 2). The TSN, operated by the CWB, consists of 78 short-period seismic stations that monitor earthquake activities over the entire island of Taiwan and its vicinity. All arrival times and earthquake location files from 1991 to 2002 reported by the CWB have been collected and analysed in this study. A few criteria are first applied to assure the selection of high-quality arrival time data and to achieve evenly distributed seismic sources. The first criterion is that the events must have been reported with more than 10 high-quality *P* arrivals (weight 0 or 1) and more than five high-quality *S* arrivals (weight 0, 1 or 2). Event–station pairs with an epicentre distance greater than 140 km are not used to satisfy the flat Earth assumption (Snoke & Lahr 2001). Traveltime data with large residuals (e.g. observed minus calculated traveltime >2 s) have been excluded. The 1-D *P*-wave velocity model of Y. L. Chen (1995) was used initially for a preliminary traveltime calculation. Earthquakes far away from the seismic network were also excluded to avoid large uncertainties on earthquake locations and model parameters. A total of 17 979 events satisfy the criteria mentioned above. Then, a horizontal grid model with about 2 km $\times$ 2 km cell size was designed and the two events recorded by the most stations were selected inside each cell. In total, 6285 events recorded by 78 stations with 69 758 *P*-arrival times and 42 733 *S*-arrival times were selected (Fig. 2). The selected 6285 events constitute less than 5 per cent of the locatable earthquakes in the original CWB catalogue.

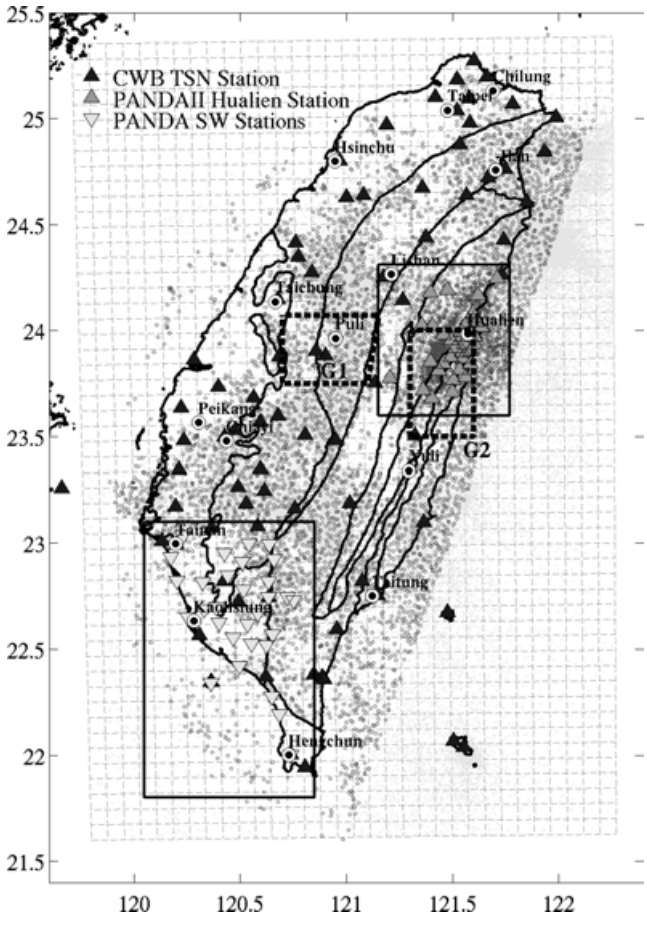

Figure 2. Locations of seismic network stations used in this study including CWB–TSN (solid triangle), PANDA II–Hualien (grey triangle) and PANDA–Pingtung (inverted triangle). Grey dots in the background are earthquake locations determined by the CWB from 1991 to 2002. Darker open circles are earthquake locations selected for this study. Areas of two dense seismic arrays are marked by squares. Areas for the selected G1 and G2 earthquake clusters are shown with dotted boxes. 3-D velocity grids with an 8 km horizontal dimension are shown in the background with dashed lines.

From 1993 to 1995, a portable seismic array (PANDA II) with 30 three-component short-period seismic stations was deployed in the Hualien area of central eastern Taiwan for 30 months in a joint project conducted by the Institute of Earth Science, the Academia Sinica and the Center for Earthquake Research and Information of the University of Memphis (Chen 1995a). Some stations were relocated during the deployment period, which increased the number of sites occupied by the PANDA II stations to 35. After removing low-quality events, 17 461 *P* arrivals and 10 003 *S* arrivals from 1218 events were also selected.

Between 1995 and 1997, 30 PANDA stations were deployed by the National Central University in the Kaoshiung-Pingtung region in southwestern Taiwan (Chen *et al.* 1998). In total, 1041 *P* arrivals and 786 *S* arrivals from 80 events recorded by the PANDA stations were selected for this study. About 87 per cent of the selected earthquakes occurred at depths shallower than 35 km. The remaining 13 per cent are deeper earthquakes that are either associated with the two subduction zones in northeastern and southern Taiwan or with the collision zone in central eastern Taiwan. While the crustal earthquakes provide excellent spatial resolution for the upper and mid crust, the deeper earthquakes provide

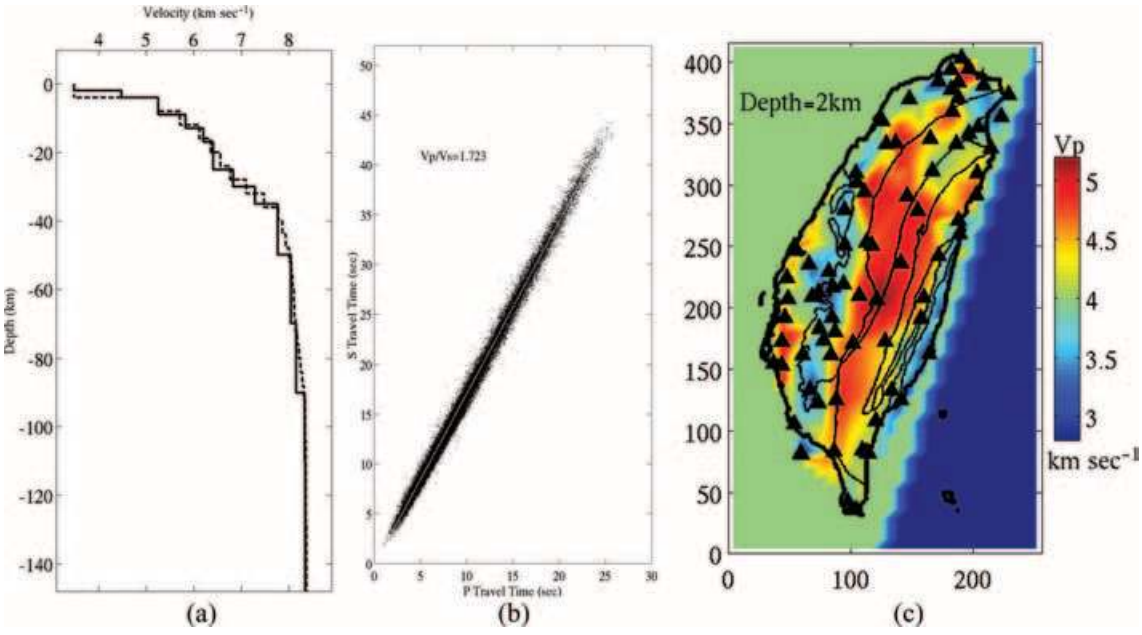

Figure 3. (a) V_P models as a function of depth showing the model of Chen (1995b) (solid line) and the interpolated starting model (dashed line). (b) A regional V_P/V_S ratio of 1.723 is determined from a least square fit of *P*-wave versus *S*-wave traveltimes. The initial V_S model is obtained by assuming a constant V_P/V_S ratio. (c) A thin-sliced revised initial 3-D velocity model at 2 km depth. The velocities in the uppermost 6 km are revised according to the observed arrival time residuals from five crustal earthquake clusters in various regions (Kim 2003). The pattern of arrival time residuals is consistent with the observed surface geology as well as the JHD *P* and *S* station corrections.

important seismic ray paths to sample the lower crust and upper mantle.

Quantification of the lateral structural variations and the design of initial velocity models

Previous studies of seismic tomography suggested that a reliable starting model is one of the most important factors for a reliable velocity inversion (Kissling 1988). In addition, seismic ray paths in the uppermost crust beneath any seismic station are mostly parallel to each other due to the nature of lower velocity at shallower depth than that at deeper depth. Therefore, there may be abundant seismic ray paths but the spatial resolution of seismic tomography is poor at shallow depth. It is, therefore, essential to determine the optimal starting models to include as much *a priori* shallow structural information as possible for a reliable inversion.

To examine and verify the importance of the starting models in the tomographic inversion, two different initial models were designed and tested using the same arrival time data. The first initial 3-D model was constructed based on a 1-D horizontally layered *P*-wave velocity model proposed by Chen (1995b) and a V_P/V_S ratio determined from the analysis of Wadati diagrams (Fig. 3). The second initial velocity model was constructed by modifying the first initial model to include the better-known shallow subsurface velocity and geology structure. There are remarkable lateral geological and structural variations across different tectonic units in the Taiwan region as inferred from the surface geology (Ho 1999), shallow seismic profiles, arrival time residual patterns from local and regional earthquakes (Chen *et al.* 1998), the distribution of arrival time residuals from antipole earthquakes (Huang 1998) and *P*- and *S*-wave station corrections from the JHD analysis (Chen 1995a; Kim 2003). The pattern of arrival time residuals derived from the uniformly distributed local earthquakes correlates well with surface geology and is similar to those of the *P*- and *S*-wave station corrections obtained from JHD analysis of five widely distributed groups of clustered earthquakes (Kim 2003). The similar patterns of *P*- and *S*-wave station corrections from crustal earthquake clusters distributed widely apart in the Taiwan region and their excellent spatial correlations with the surface geology and tectonic units suggest that lateral structural variations in the uppermost crust in Taiwan must be responsible for the observed traveltime corrections (Kim 2003). Therefore, V_P and V_S in the uppermost 6 km of the second initial velocity model has been adjusted to accommodate the observed traveltime residuals and station corrections.

Using the same traveltime data, the application of the second initial velocity model resulted in an improvement of about 10 per cent in the arrival time RMS (root-mean-square) residuals for *P* and *S* waves in the final 3-D tomographic inversion with respect to those obtained using the first initial model. Thus, the second initial velocity model was used for the 3-D tomographic inversion discussed in this paper. Our preferred initial velocity model can be improved in the future when more reliable *a priori* information is available, for example, from direct measurements from boreholes, or from shallow seismic profiles, or from other geophysical methods.

Design of a 3-D grid model

The study area is defined by a box that extends 256 km in the east–west direction, 416 km in the north–south direction and 152 km in depth with 4 km above and 148 km below sea level. The model area has been parametrized by 8 km × 8 km × 2 km blocks for velocity inversion and 2 km × 2 km × 2 km blocks for the forward traveltime calculation. The block size is determined based on the station–source configuration and the maximum available memory size and speed of the computer we used. The smaller block size for

traveltime calculation is adopted to improve spatial resolution for traveltime calculation through 3-D velocity models. The coordinates in this paper are given in kilometres east and north from a reference point at 119.8°E and 21.6°N.

Damping and smoothing

Damping and smoothing values have to be carefully selected to find an optimized inversion and to achieve realistic 3-D structural models. Selection of a very large damping value would result in small model variance, while an extremely small damping value would cause the velocity model to oscillate from one block to the next. An appropriate smoothing is required for a stable inversion. The speed of convergence towards the final solution over iterations has also been considered. If the convergence is slow, a sequential inversion would be an efficient approximation for a simultaneous inversion of *P*- and *S*-velocity models and hypocentre parameters. The slow approach scheme will also produce a final model less dependent on the starting velocity model. There is no simple way to determine the best damping–smoothing pair. It is also very difficult to separate their effects because they are coupled together during inversion. An optimal pair of damping and smoothing can be selected based on trial and error using the selected data set previously described. A series of one-iteration inversions with different damping values have been performed. After one iteration, arrival time RMS reduction and model variance for *P* and *S* waves have been computed. Our observations reveal that large damping has resulted in small model variance, while small damping has caused a significant model variance without significant RMS reduction (Fig. 4). Thus a *P*-wave inversion damping of 50 and a *S*-wave inversion damping of 20 have been selected, which have achieved the biggest RMS reduction without significant model variance. Relatively small model variance will ensure a slow approach to reach to the final solution over iterations. This procedure for selecting the damping value is similar to the method proposed by Eberhart-Phillips (1986). A large smoothing value of 128 has been chosen to stabilize the inversion procedure during the first few iterations. Once large-scale structures are outlined and resolved after the first few iterations, the smoothing value is then gradually reduced throughout the rest of iterations to approach to the final model. With the properly selected damping and smoothing processes in this study, the *P* and *S* arrival time RMS residuals decreased from the initial 0.58 and 0.67 s to 0.15 and 0.21 s, respectively, after 20 iterations. This represents a 74 per cent and 69 per cent reduction of arrival time RMS residuals for *P* and *S* waves, respectively and the inversion is converged.

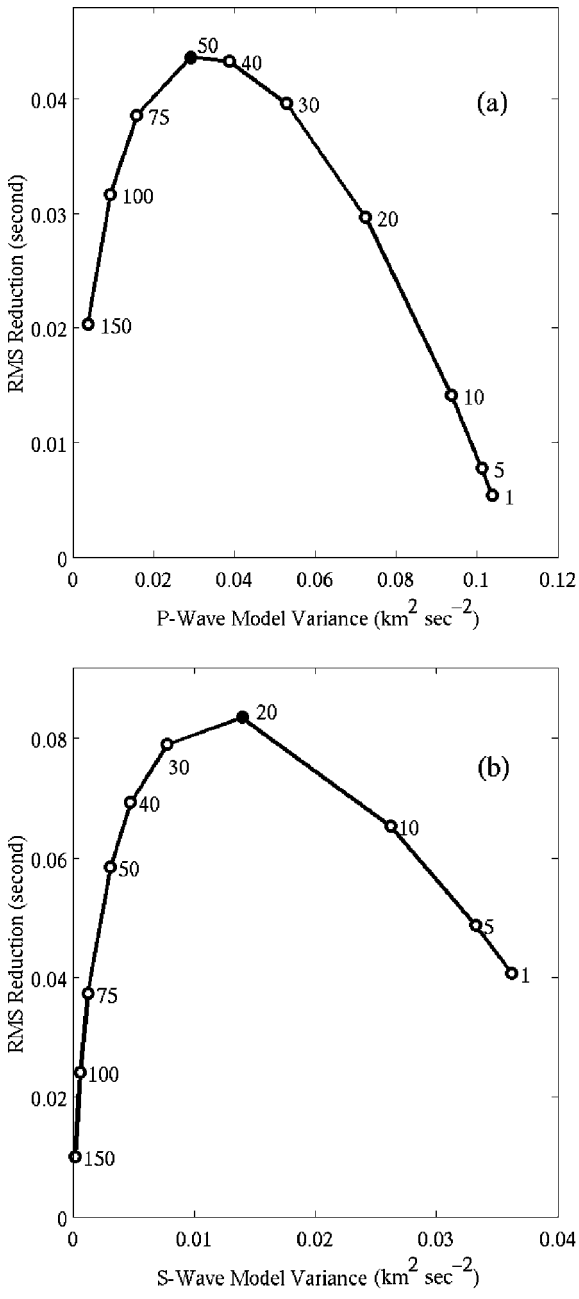

Figure 4. Trade-off curves to select optimum damping values for (a) *P*-wave and (b) *S*-wave tomography inversions. Model variances and traveltime RMS reductions are calculated after one iteration with the given damping values (shown to the right of the open circles). Small damping has caused large model variance without significant RMS reduction. An extremely large damping value results in a very small model variance and small RMS reduction. Different damping values of 50 and 20 are selected for *P*- and *S*-wave inversion, respectively, which have produced the most significant RMS reduction without causing large model variances (shown by the solid circles).

RESULTS AND DISCUSSIONS

Synthetic tests

Estimates of model resolution and model uncertainty are critically important in any tomographic inversion. Primary factors controlling these estimates are the source–receiver geometry and parametrization of the model that defines how well the model is sampled (Benz *et al.* 1996). Two synthetic tests are performed to qualitatively estimate resolution, uncertainty and similarity of the resolved images to the real Earth. Following Zhao *et al.* (1992) and Hole *et al.* (2000), the checkerboard resolution test (CRT) and the restoring resolution test (RRT) were carried out to examine how much the original velocity images can be retrieved from the inversion. Details of the synthetic test results can be found at Kim (2003).

The CRT can be applied to explore the spatial resolution from the existing ray coverage. 3-D *P*- and *S*-wave checkerboard velocity models were constructed by adding ± 0.3 km s^{-1} of lateral velocity variations to the horizontally homogeneous velocity models with 32 km in the horizontal dimension and 8 km in the vertical dimension, corresponding to $4 \times 4 \times 4$ blocks in a checkerboard box. Therefore, a 0.6 km s^{-1} velocity discontinuity across the

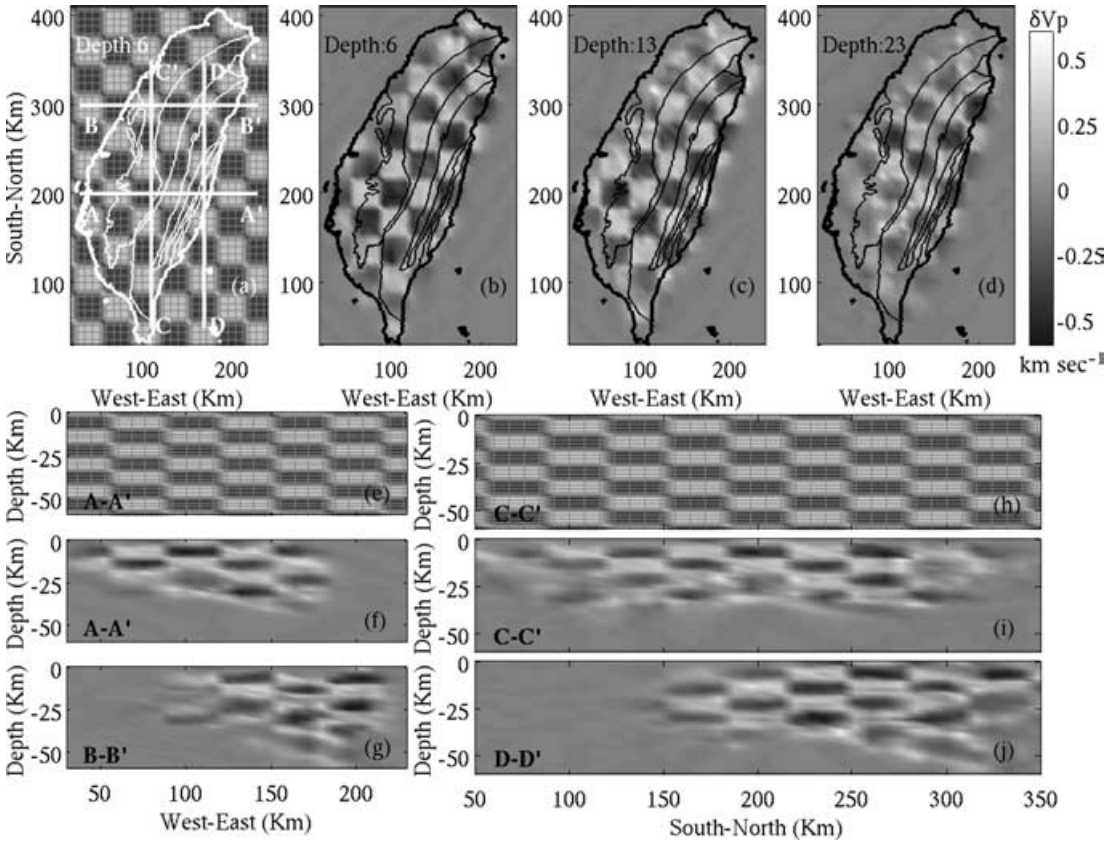

Figure 5. Results of the checkerboard resolution test (CRT) for *P* waves. There are 4 × 4 × 4 blocks (block size 8 km × 8 km × 2 km) in a checkerboard box, corresponding to 32 km and 8 km in horizontal and vertical dimensions, respectively. Horizontal slices show (a) the original checkerboard velocity pattern at 6 km depth, (b, c, d) the recovered checkerboard velocity patterns at selected depths shown at the upper-left corner of each slice. West–east trending vertical slices show (e) the original checkerboard along A–A′ and (f, g) the recovered checkerboard patterns along A–A′ and B–B′, respectively. South–north trending vertical slices show (h) the original checkerboard along C–C′, and (i, j) the recovered checkerboard patterns along C–C′ and D–D′, respectively. Checkerboard patterns have been successfully recovered as deep as 25–30 km where cells are covered by many rays.

boundary of checkerboard boxes is introduced to simulate large lateral velocity variations expected in the Taiwan area. Synthetic traveltimes were calculated from the selected hypocentres to all surface stations across the checkerboard velocity models. Then the synthetic data were inverted using the same procedures applied to the actual data using homogeneous initial models. A few selected horizontal and vertical slices of the original checkerboard pattern and the recovered velocity models for V_P and V_S are shown in Figs 5 and 6, respectively. Cumulative ray lengths in each cell at the last iteration are presented in Fig. 7. The distribution of ray coverage and the recovery of checkerboard pattern at depths shallower than 4 km are poor due to the facts that ray paths are along the same upward directions and are limited to the vicinity beneath seismic stations. More than 93 per cent of the original velocity patterns have been successfully recovered at least to a depth of 25 to 30 km for most blocks with cumulative ray length more than 30 km (≈10 rays). Beyond this depth, the ray path coverage as well as the resolution to recover the original velocity patterns is not as uniformly distributed as that above. Kim (2003) has also tested with various checkerboard sizes and found similar results.

The RRT is used to inspect how the resolution of the inverted images is affected by errors or noises in the data. Typical errors include, for example, the picking uncertainties for the *P* and *S* arrival times. Kim (2003) tested RRT and concluded that the complicated crust and upper mantle structure models in the Taiwan region can be successfully retrieved from the configuration of the existing station location and the distribution of background seismicity.

Validation of the 3-D velocity models using the JHD technique

The resultant 3-D velocity models are further validated following the approach proposed by Pujol (1995, 2000) using the JHD technique. The JHD technique is applied to the observed data and to a set of synthetic arrival time data generated from the resultant 3-D velocity models. If the resultant 3-D velocity models are compatible with the real Earth, the observed and synthetic JHD locations and station corrections are expected to be similar. Otherwise, the resultant 3-D models should be viewed with caution. From Kim (2003), the JHD *P*- and *S*-wave station corrections for the observed and synthetic arrival time data from G1 and G2 earthquake clusters (Fig. 2) are shown in Figs 8 and 9, respectively. The magnitude and pattern of the observed station corrections from the two widely separated earthquake clusters are similar, suggesting that the uppermost crust, where the majority of the ray paths from the two clusters overlap, must be responsible for the generation of the observed station corrections. They further reveal that not only are there excellent spatial correlations between the contour lines of the station corrections and the regional tectonic boundaries, but there are also drastic patterns of negative corrections for stations in the Central Mountain

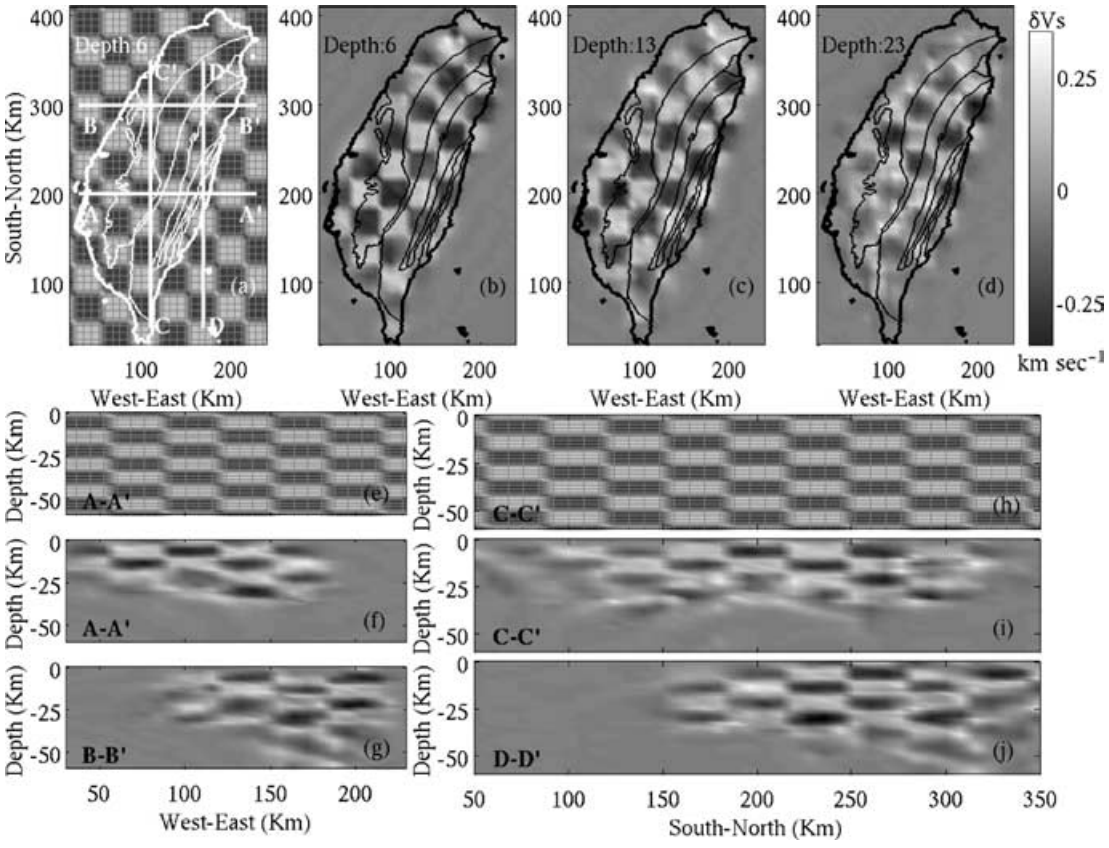

Figure 6. Similar to Fig. 5 for *S* waves. The resolution of checkerboard recovery pattern at deeper depths is slightly lower than that of *P* waves.

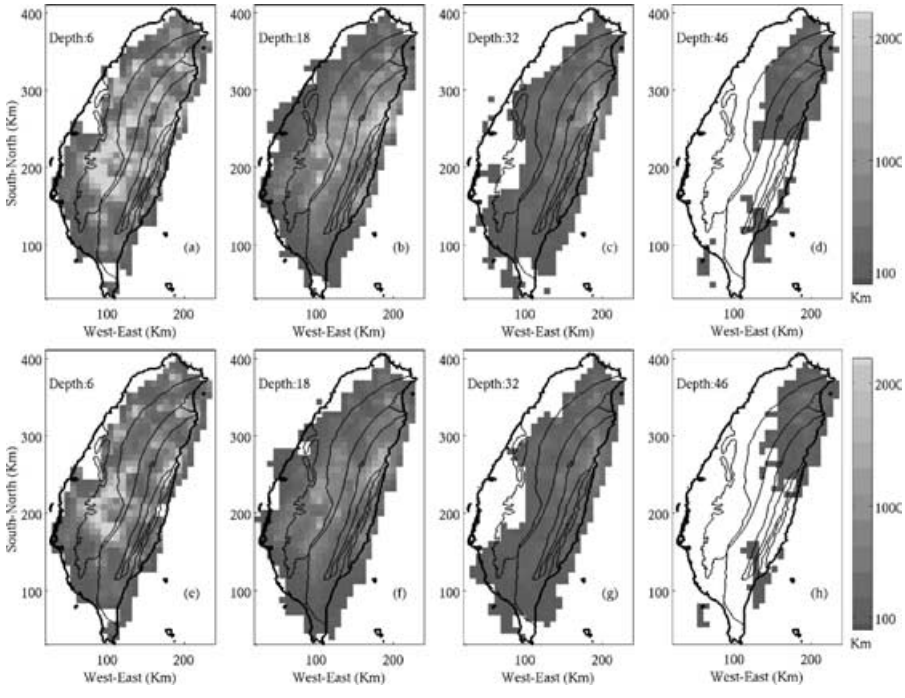

Figure 7. Display of cumulative ray lengths during the last iteration at selected depths (shown on the upper-left corner): (a–d) for *P* waves and (e–h) for *S* waves. The depth of the horizontal slice is shown on the upper-left corner.

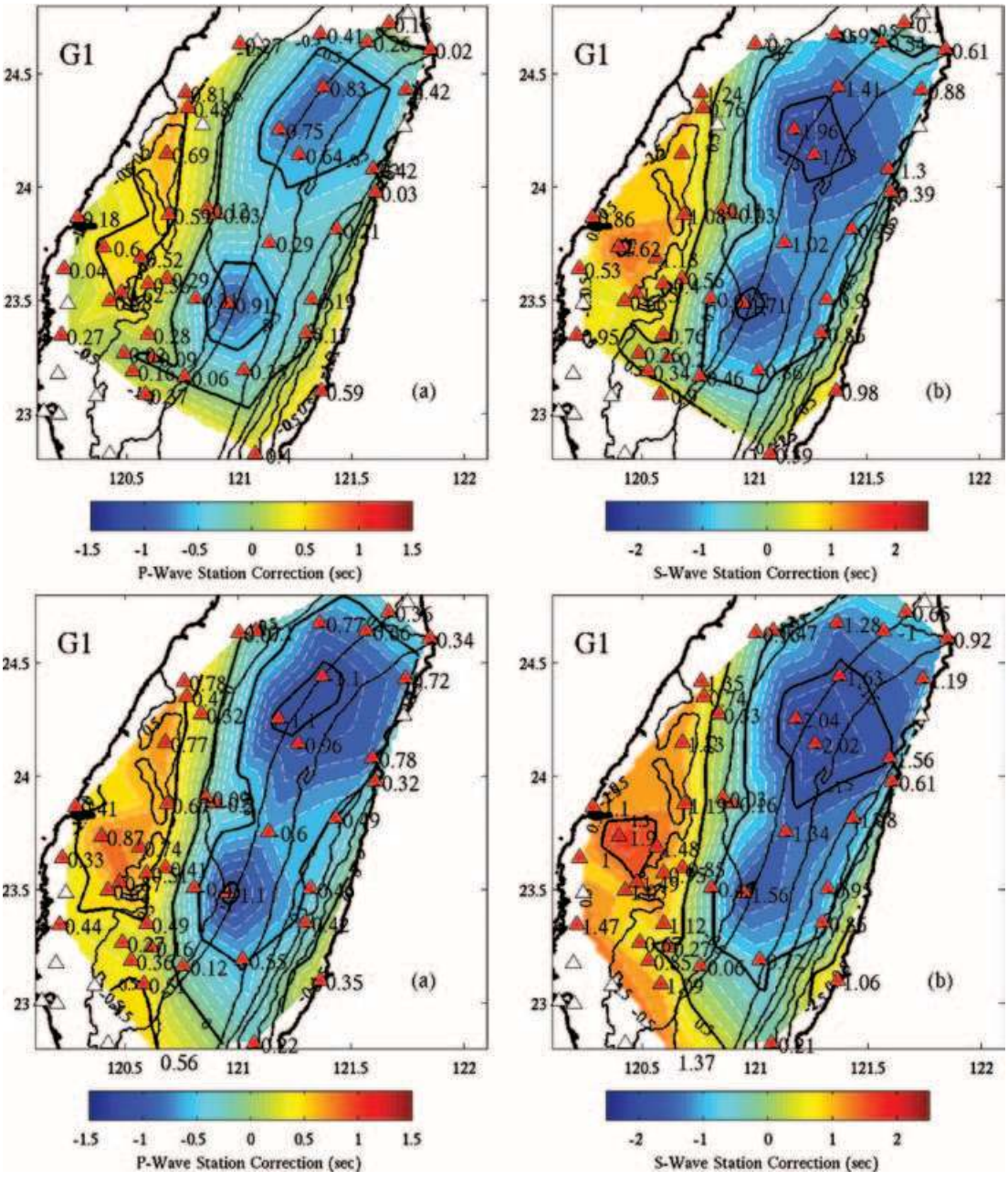

Figure 8. Distribution of the observed (top) and synthetic (bottom) JHD station corrections for *P* (left) and *S* waves (right) determined using selected earthquake clusters in Group 1 (G1 in Fig. 2).

Range, and positive corrections for the stations in the Western Foothills and Coastal Plain. The negative station corrections imply the existence of higher-velocity materials in the upper crust beneath the Central Mountain Range, while the positive corrections indicate the existence of lower-velocity material beneath the Western Foothills and Coastal Plain. Most importantly, the similarity of *P*- and *S*-station corrections between the observed and the synthetic data confirms that the resultant 3-D V_P and V_S models derived from the tomographic inversion should be close to the real Earth structure beneath Taiwan. Thus, the resultant 3-D models as shown in Fig. 10 for a few thin-sliced horizontal sections at various depths can be explored to correlate structures and earthquakes in the Taiwan region.

Lateral variation of the Moho configuration

The depth to the Moho is about 35 km beneath the Coastal Plain in western Taiwan (Fig. 11). The Moho depth increases rapidly toward the east and reaches its maximum depth of ~55 km beneath the eastern Central Mountain Range (Fig. 11). A rapid decrease of the thickness of the crust is observed immediately across the Longitudinal Valley to the Coastal Mountain Range. In general, the east–west variation of the Moho depths observed in this study is similar to those reported in a few previous studies (Roecker *et al.* 1987; Roecker 1993; Rau & Wu 1995; Shih *et al.* 1998; Yeh *et al.* 1998) although there are some minor differences at depth. It is, however, substantially different from the crustal thickness suggested by

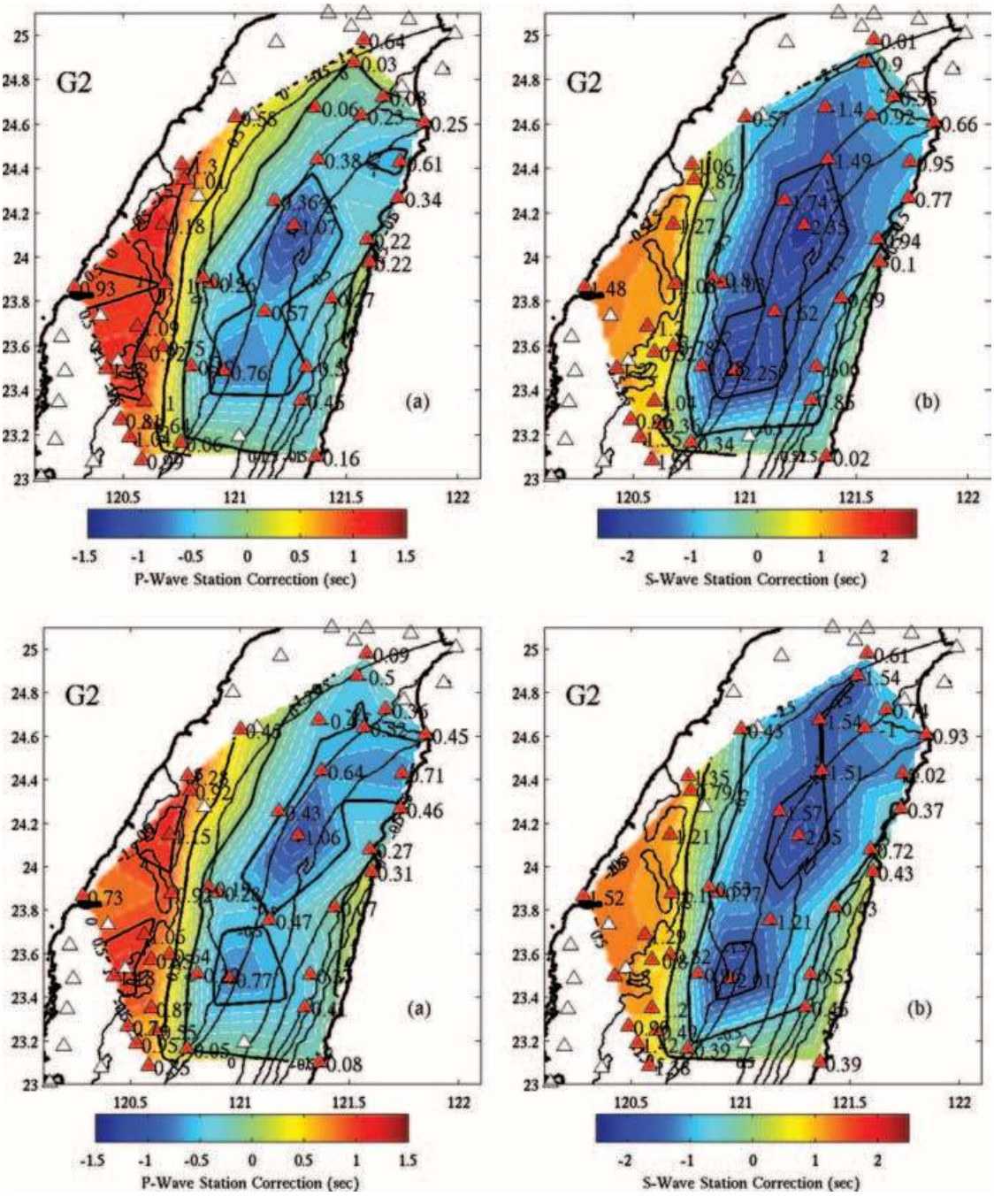

Figure 9. Similar to Fig. 8 for Group 2 (G2 in Fig. 2).

Ma *et al.* (1996), where a Moho depth of 30–35 km was estimated beneath the Central Mountain Range. The thickest crust appears to be located beneath the Central Mountain Range in central Taiwan where the most advanced collision tectonics took place. Relatively sharp and thin crust–mantle transitional boundaries can be observed beneath western Taiwan as shown in a few east–west cross-sections across Taiwan, while thicker crust–mantle transition layers are observed beneath the Central Mountain Range (Fig. 11). It is possible that the thinner transition layers beneath western Taiwan in the 3-D velocity images may be a result of low resolution in inversion due to poor sampling of seismic rays across lower crust and upper mantle.

Images of sedimentary basins

It is commonly recognized that resolution of the uppermost few blocks in the 3-D models derived by inversion may be poor because of almost parallel ray paths in those blocks. In such a case, a 3-D tomographic inversion with a homogeneous initial model may easily transfer the traveltime variations that may exist in the uppermost few blocks into deeper blocks, thus introducing incorrect images into the resultant velocity models. However, with *a priori* information of the lateral structural variations included in the initial model as shown in this study, critical structure information in the upper few blocks or upper crust may have a better chance of

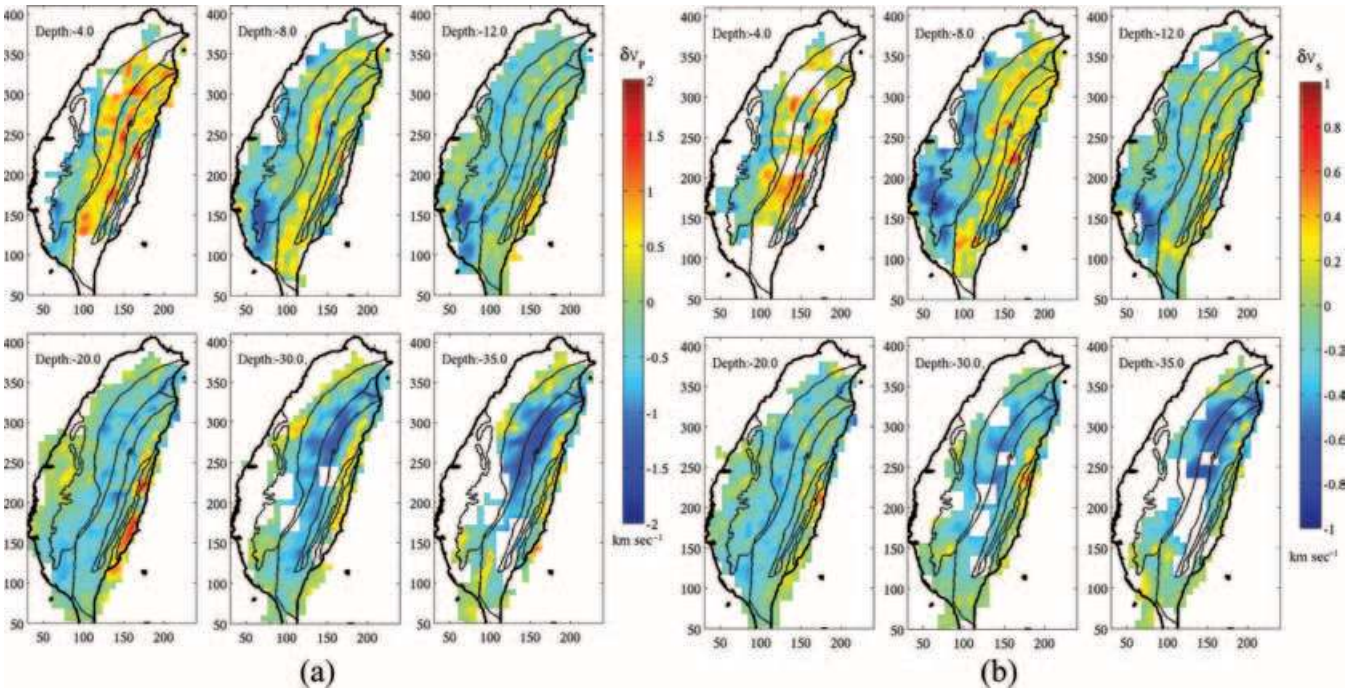

Figure 10. Map views of horizontally sliced (a) *P*-wave velocity anomalies and (b) *S*-wave velocity anomalies at selected depths. Low-velocity anomalies at shallow depth beneath western Taiwan can be associated with thick basins. The Central Mountain Range is characterized by an anomalous high-velocity upper crust and low-velocity mid to lower crust for both *P* and *S* waves. It is apparent that patterns of subsurface velocity anomalies resemble major geological divisions observed on the surface.

being resolved. The thin-sliced velocity images shown in Fig. 12 clearly demonstrate that many low-velocity sedimentary basins in the Taiwan region have been resolved from a careful design of initial models in the tomographic inversion. Further detailed information for these near surface low-velocity basin structures can be found in Kim (2003).

Collision zone in central eastern Taiwan

The thick crust beneath the Central Mountain Range seems to transfer rapidly to thinner crust beneath the Longitudinal Valley and Coastal Range (Fig. 11). A high-velocity region (>7.5 km s^{-1}) is observed at a depth of ∼15 km beneath the Longitudinal Valley, which is probably associated with the oceanic upper mantle. In the modelling of anomalous *Pn* waves from an earthquake near the Hualien region observed at stations as close as 60 km along the Longitudinal Valley, Liang & Chiu (2005) provided further evidence that the Moho depth beneath the Longitudinal Valley must be very shallow (∼15 km). Near the Taitung region in southeastern Taiwan, where the collision is in its early stage, the southern collision zone is characterized by a well-defined eastward dipping seismic zone extending from near the surface to ∼25 km depth, a vertical seismic zone associated with the eastern Longitudinal Valley Fault, and a previously unknown northeast–southwest trending fault inside the Central Mountain Range (Fig. 13). The eastward dipping seismic zone is located within a region of low V_P, and high V_P/V_S ratio corresponding to a highly fractured or water-saturated transition region. In the Hualien region in central eastern Taiwan, where the collision is in its most advanced stage, the collision zone is characterized by a steeply westward dipping seismic zone extending from near the surface to ∼30 km (Fig. 14). This active seismic zone separates the typical continental crust to the west and the oceanic crust to the east marking the eastern boundary fault of the Central Mountain Range in central Taiwan. More detailed discussions of the collision zone structures are reported in two other papers (Kim *et al.* 2005a,b).

Subduction zone in northeastern Taiwan

The tectonic structures in the Taiwan region are further complicated by the crust and upper mantle deformation associated with the two subduction zones, one in northeastern Taiwan and the other in southern Taiwan. Since there are not enough data from very few seismic stations in southern Taiwan to allow a reliable image of the southern subduction zone, only the subduction system in northeastern Taiwan is briefly described here. In a map view, a NNW–SSE line extending from Hualien to Taipei clearly marks the western termination of the intermediate-depth earthquakes, a clear indication of the western extent of the subducting oceanic plate (Fig. 15). The geometry of the subducting Philippine Sea Plate can be clearly defined from the relocated hypocentres (Fig. 16). A significant thin zone of low V_P extending to a depth of 80 km can also be clearly identified just above the subducting slab beneath northern Taiwan.

Tatun-Chilung volcano group

The spatial resolution of the 3-D tomographic inversion near the Tatun-Chilung volcano group in northern Taiwan may be very limited because the area is near to the edge of the permanent seismic network. However, results of the tomographic inversion indicate that a region of low V_P, low V_S, and a slightly high V_P/V_S ratio can be identified at depths from 5 to 10 km beneath the volcanic zones (Fig. 17). If a partially molten magmatic source exists, we would expect the region to be characterized by lower V_P and V_S. As the degree of partial melting increases, we would expect V_S to decrease faster than V_P and thus lead to a higher V_P/V_S ratio. Therefore, the observed velocity structure images beneath the Tatun-Chilung volcano group may imply the existence of partially molten materials

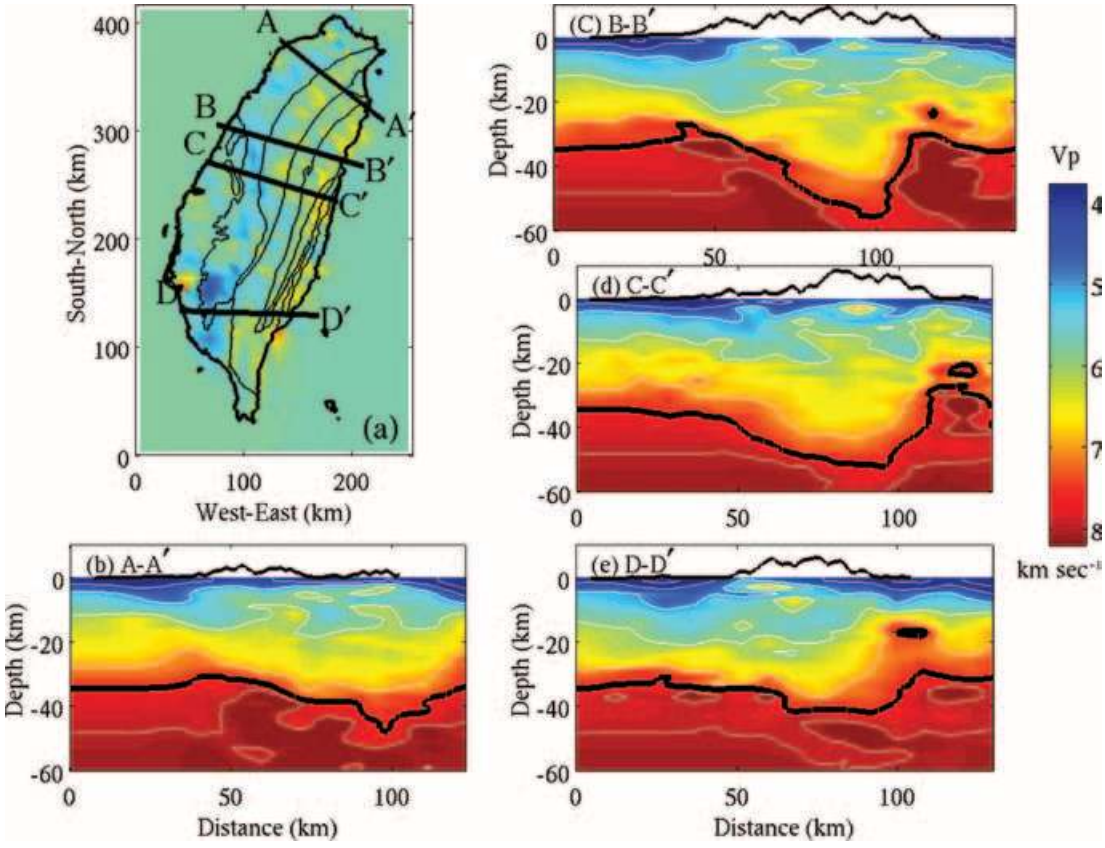

Figure 11. Cross-sectional views of the velocity model beneath Taiwan Island showing the lateral variation of crustal structure and the Moho depth. The 7.8 km s^{-1} contour line is marked with a solid black line. In general, the Moho depth thickens beneath the Central Mountain Range. It reaches its maximum depth, i.e. 55 to 60 km, beneath the eastern Central Mountain Range in central Taiwan, where collision tectonics is dominant. Surface elevation has been vertically exaggerated (×3) to show elevation. The crust in northern and southern Taiwan (A–A′ and D–D′) beneath the Central Mountain Ranges is not as thick as that in central Taiwan.

or a magma reservoir at depth, even though volcanism in this region ceased in the Pliocene (Ho 1999). Two steeply dipping seismic zones can be defined extending from near the surface to the anomalous low V_P and high V_P/V_S region. These two seismic zones may mark the upward paths or the 'conduits' of the magmatic materials from deeper depths. Further seismogenic study of Tatun-Chilung volcano region is reported in another paper (Kim *et al.* 2005c).

Velocity structure and crustal seismicity beneath central western Taiwan

The crustal seismicity in central western Taiwan can be divided into two groups, i.e. upper and lower crust seismicity, separated by a less seismic mid-crust. A scattered trend of gently east dipping seismicity can be seen in the lower crust starting from ∼20 km depth near the west coast to ∼50 km beneath the western Central Mountain Range (Fig. 18a). This deep seismic zone is located along the transitional boundary between the eastward dipping lower crust and the upper mantle. Since seismicity along this deep zone does not seem to extend beyond the bottom of the Central Mountain Range, internal deformation associated with earthquakes in this deep zone is presumably related to the deformation related to the convergence and thickening of the Eurasia Plate approaching the collision zone. The hot, aseismic, thick and wide mid to lower crust beneath the Central Mountain Range may serve as a backstop separating the deep seismic zones between western and eastern Taiwan. Upper crust seismicity in central western Taiwan is confined mainly to an east–west trending horizontal zone at depths shallower than ∼15 km that ruptured during the 1999 Chi-Chi earthquake. However, the eastward propagation of aftershocks along the subhorizontal zone was apparently interrupted by a steeply westward dipping seismic zone beneath the western Central Mountain Range. This steeply dipping seismic zone, activated during the 1999 Chi-Chi earthquake sequence and extending to a depth of ∼30 km (Chen *et al.* 2002), is apparently a major boundary separating the deformed structural features and their associated seismicity beneath central western Taiwan and the Central Mountain Range. Shallow earthquakes and their associated deformation in western central Taiwan seem to correlate well and continue into Central Mountain Range, indicating that upper crust deformation across the entire east–west section of Taiwan can be closely related to the plate collision and plate convergence initiated along the collision suture in eastern Taiwan.

Anomalous velocity variations and seismicity beneath the Central Mountain Range

The 3-D velocity model and relocated seismicity in the central Taiwan region has been summarized in the cross-sectional view shown in Fig. 18. At depths shallower than 15 km the uppermost crust of the Central Mountain Range is characterized by high-velocity anomalies ($\Delta V_P \sim +1.0$ km s^{-1} and $\Delta V_S \sim +0.6$ km s^{-1}) as shown in a few thin horizontal slices at various depths (Fig. 10) and a few cross-sectional views (Fig. 11). Highly metamorphosed rocks observed at the surface of the Central Mountain Range contribute to

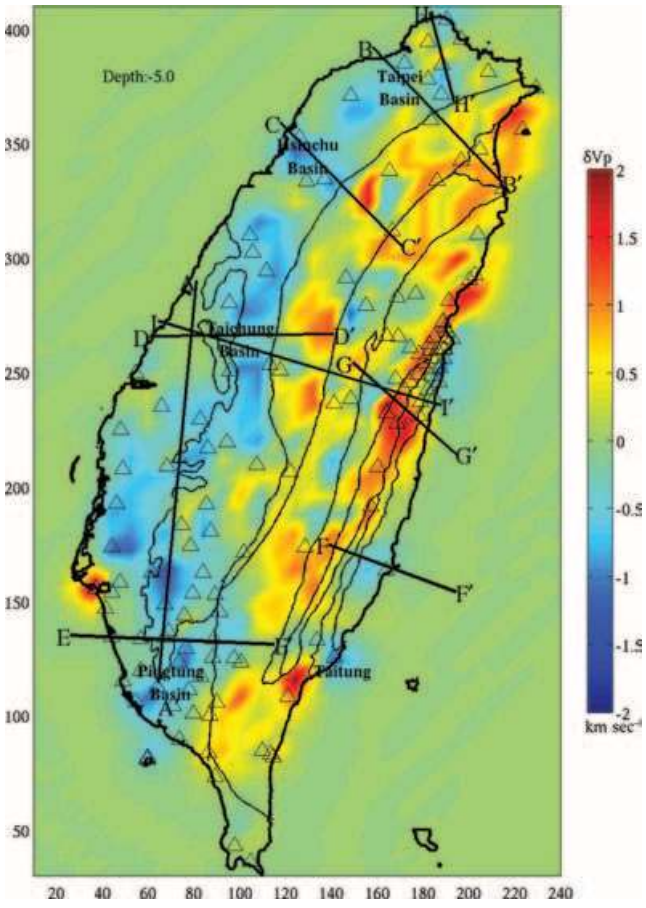

Figure 12. Map view of a horizontally thin-sliced *P*-wave velocity anomaly at 5 km depth showing clearly that major sedimentary basins in the Taiwan area are characterized by images of low-velocity anomalies. Open triangles mark the location of seismic stations.

these high-velocity anomalies. Shallow earthquakes in the Central Mountain Range are confined mainly to the upper 15 km of high-velocity crust (Fig. 18a). Within the brittle upper crust, seismicity is not uniformly laterally continuous. A few apparently aseismic regions or breaks in the upper crust may correspond to the areas of high geothermal activity where hot springs are commonly observed. In contrast, the deeper portion of the Central Mountain Range (>15 km) is characterized by low-velocity anomalies ($\Delta V_P \sim -1.5$ km s^{-1} and $\Delta V_S \sim -0.8$ km s^{-1}) (Figs 10 and 11) and extremely low seismicity relative to the surrounding regions (Fig. 18a). The observations of extraordinarily high surface heat flow (over 400 mW m^{-2}) (Hwang & Wang 1993; Lin 2000) may suggest high temperatures at larger depths beneath the Central Mountain Range. Thus, low velocity and low seismicity in the mid to lower crust beneath the Central Mountain Range can be attributed to high temperature and high geothermal activity at depth. Excess heat energy may be supplied from the high-temperature oceanic upper mantle beneath the thin Philippine Sea Plate to the east and beneath the thick Eurasian Plate to the west (Ma *et al.* 1996), and may also be contributed by active shear heating during collision.

Boundary faults for the Central Mountain Range in central Taiwan

As shown in Fig. 18, it is apparent that the Central Mountain Range in central Taiwan is bounded by two steeply westward dipping faults that extend from near the surface to a depth of ~30 km. The eastern boundary fault near Hualien marks the transitional boundary between the thickened continental and oceanic crusts, along which high seismicity can be associated with the most advanced collision between the two plates. The western boundary fault was not active or apparent before the 1999 Chi-Chi earthquake. It was activated and formed a conjugate fault pair with a subhorizontal fault at a depth of 10 to 12 km that ruptured during the 1999 Chi-Chi main shock–aftershock sequence (Chen *et al.* 2002). Therefore, the 1999 Chi-Chi aftershock activity associated with the deformation along the 'décollement' proposed by the thin-skinned deformation model (Suppe 1987) does not seem to extend eastwards beyond this western boundary fault into the ductile mid-crust beneath the Central Mountain Range. The upper crust beneath the Central Mountain Range is characterized by high seismicity, higher seismic velocity and brittle deformation, while the mid to lower crust is aseismic and characterized by lower seismic velocity and ductile deformation. Thus, excess heat supplies to the mid to lower crust beneath

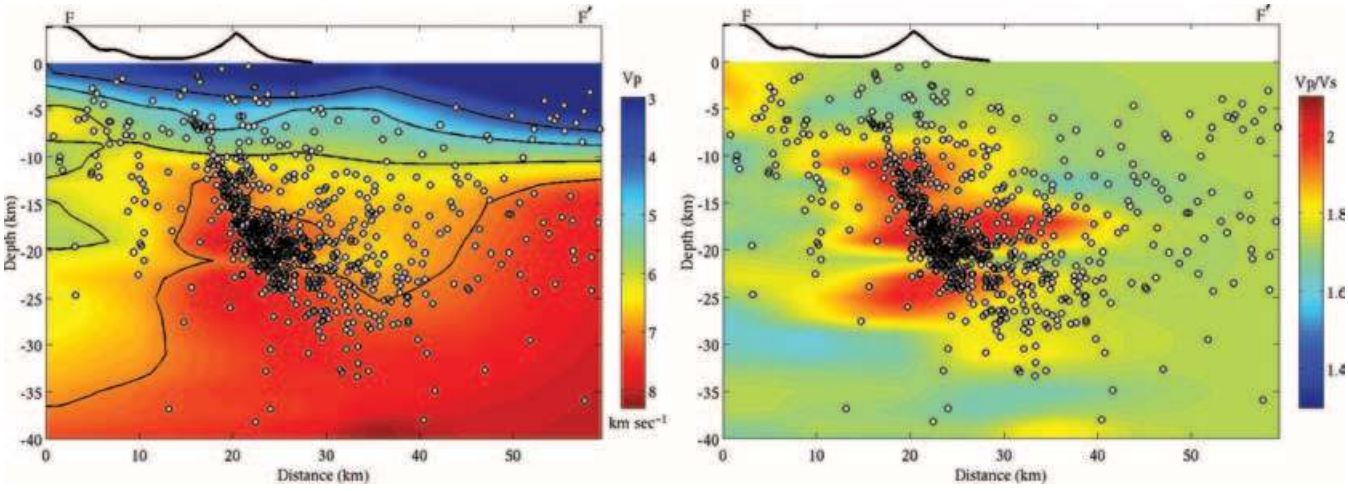

Figure 13. *P*-wave velocity profile and relocated seismicity for cross-section F–F′ (Fig. 12) near the Taitung area in the southern Longitudinal Valley. Earthquakes within ±3 km are projected onto the profile. Surface elevation is vertically exaggerated (×2). The velocity profile is contoured at 4.5, 5.5, 6.5 and 7.8 km s^{-1}. An east dipping earthquake cluster that extends to depths near 30 km can be associated with the northern extension of the Taitung Trough Fault (TTF).

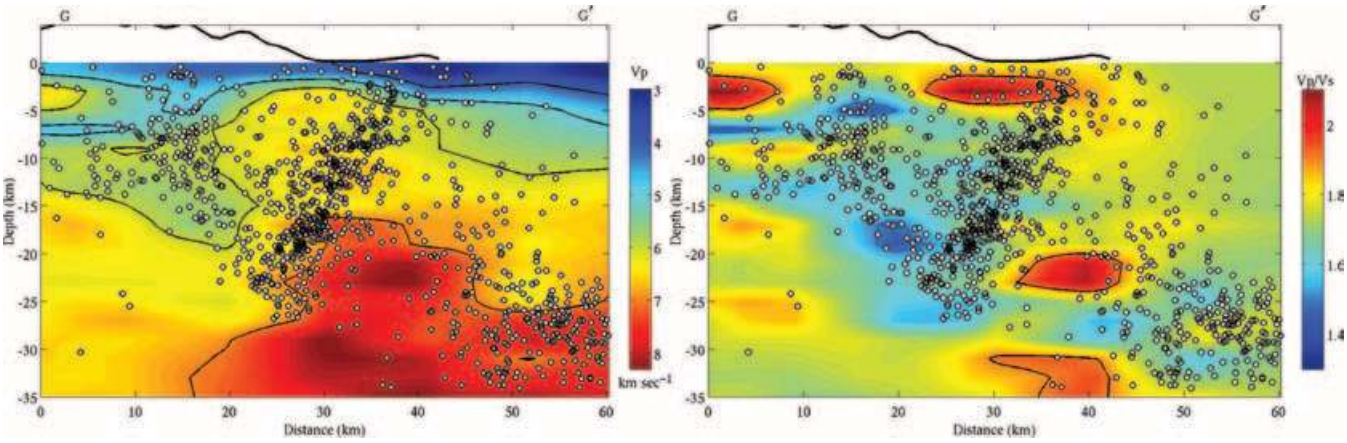

Figure 14. *P*-wave velocity profile and relocated seismicity for cross-section G–G′ (Fig. 12) near the Hualien region of the northern Longitudinal Valley. Earthquakes within ±3 km are projected onto the profile. Surface elevation is vertically exaggerated (×2). The velocity profile is contoured at 4.5, 5.5, 6.5 and 7.8 km s^{-1}. A clear linear seismicity trend from the surface to a depth of ∼30 km marks the eastern boundary fault along the eastern Longitudinal Valley.

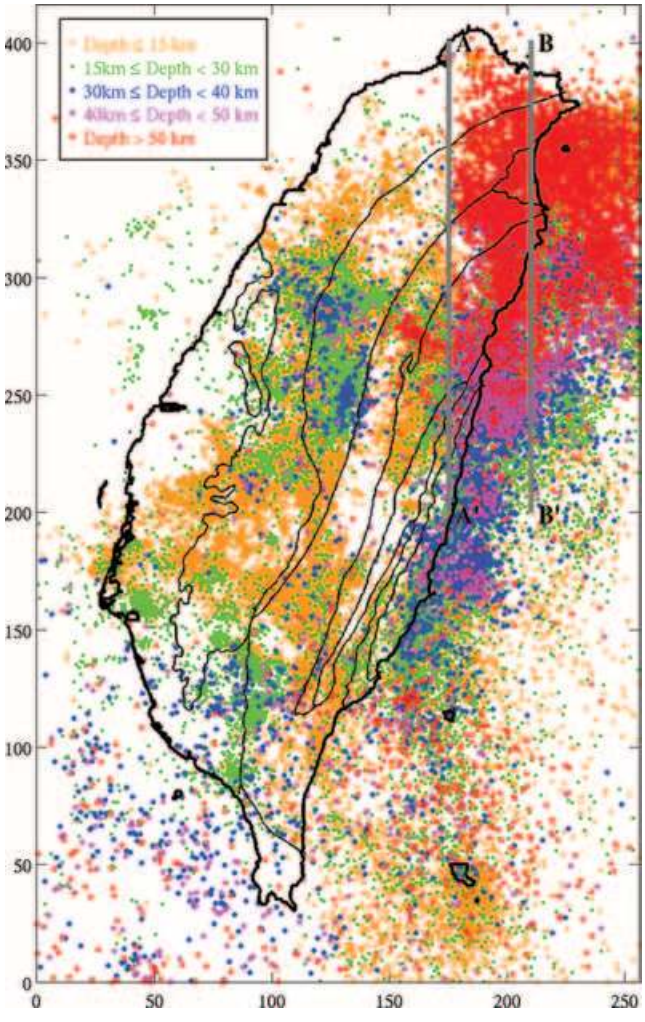

Figure 15. Relocated hypocentres in the Taiwan region using 3-D V_P and V_S models obtained from this study for the period from 1991 to 2002. The depths of the earthquakes are colour-coded. The western termination of the subduction Philippine Sea Plate in northern Taiwan can be clearly seen from the distribution of hypocentres deeper than 40 km.

the Central Mountain Range may induce high temperature and high geothermal activity so that the density of a large portion of lower crust decreases, the crust volume increases and therefore the continental crust is uplifted and thickened. While the crust beneath the Central Mountain Range uplifted and thickened, the region beneath the western Central Mountain Range and the Western Foothills is undergoing deformation associated with plate converging, crust uplifting and thickening. However, this region remained aseismic and ductile until it ruptured along the western boundary fault during the major aftershock sequence of the 1999 Chi-Chi earthquake.

Comparison of the 3-D velocity models with the results from other geophysical studies

The 3-D V_P model obtained in this study is first compared with the models obtained from two onshore/offshore wide-angle deep seismic profiles across Taiwan (Shih *et al.* 1998; Yeh *et al.* 1998). These two seismic profiles, one along the central and the other along the southern cross-island highway, were designed to sample the deeper crust and upper mantle structures beneath Taiwan using large offshore airgun arrays. Although there are relevant differences in the resolution between the results from seismic profiles and from tomographic inversion, the configurations of major deep structures are highly comparable. For instance, the geometry and depth variations of the Moho along the cross-island highway in central Taiwan (Shih *et al.* 1998) are very similar to those imaged in this study. The results of Shih *et al.* (1998) reveal that the thickness of the crust beneath the Western Foothills is only about 35 km and it increases to about 45 km beneath the eastern Central Mountain Range. Further to the east, the depth of the Moho decreases rapidly towards the Philippine Sea Plate. The other profile along the southern cross-island highway (Yeh *et al.* 1998) also shows a similar Moho geometry. In their model, the thickness of the crust reaches to about 50 km under the Central Mountain Range with a thick lower crust. Thus, the lateral variations of the Moho depth, the location of the deepest Moho and the thick lower crust beneath the Central Mountain Range derived in this study are comparable with those obtained from the onshore/offshore wide-angle deep seismic profiles.

A Bouguer gravity anomaly map based on the recent observations at 603 sites evenly distributed over the entire island of Taiwan (Yen *et al.* 1995) has provided important insights into the larger

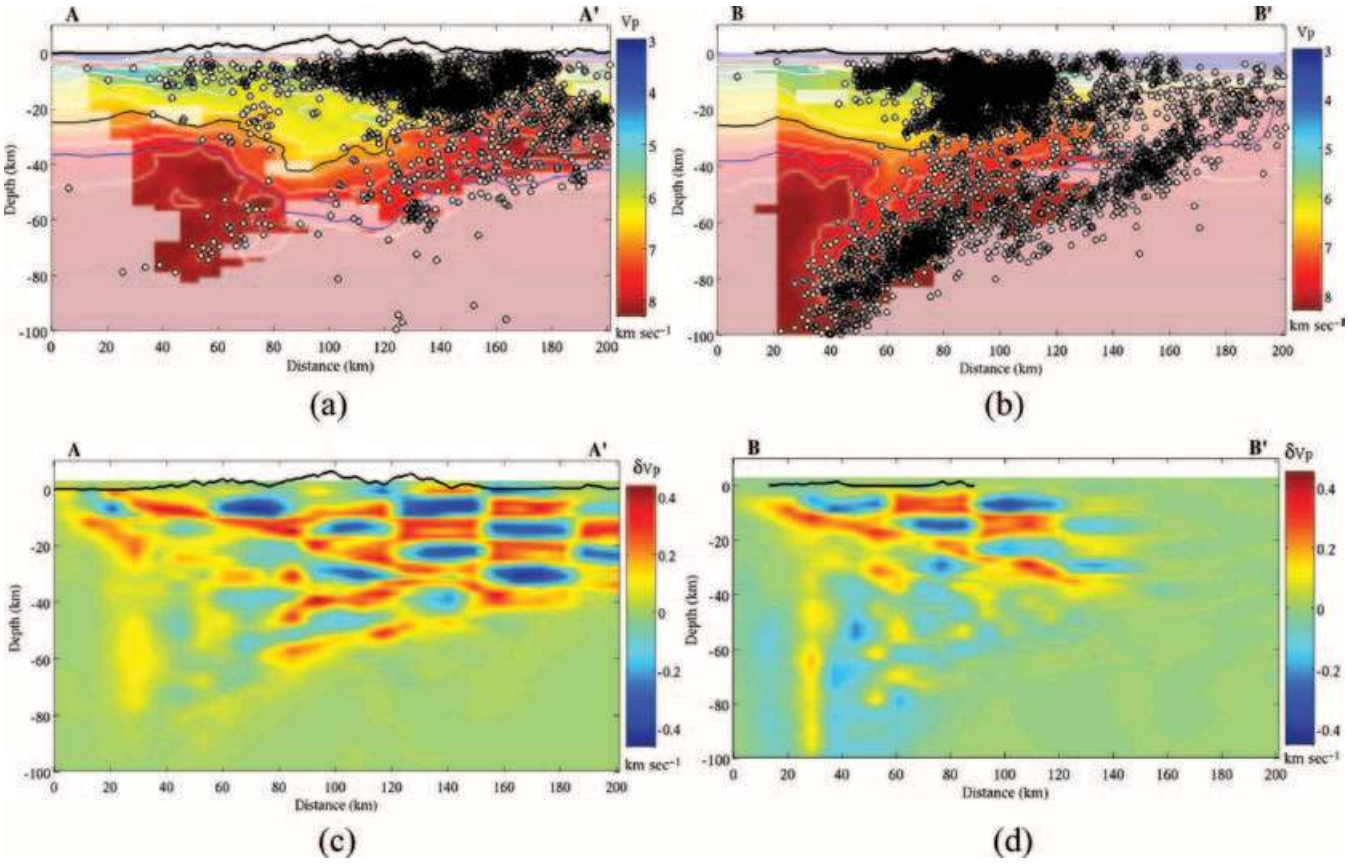

Figure 16. Subduction system in northeast Taiwan showing that the upper surface of the subducting Philippine Sea Plate can be delineated clearly by the distribution of the relocated hypocentres. A low-velocity zone can be identified immediately above the upper surface of the subducting slab.

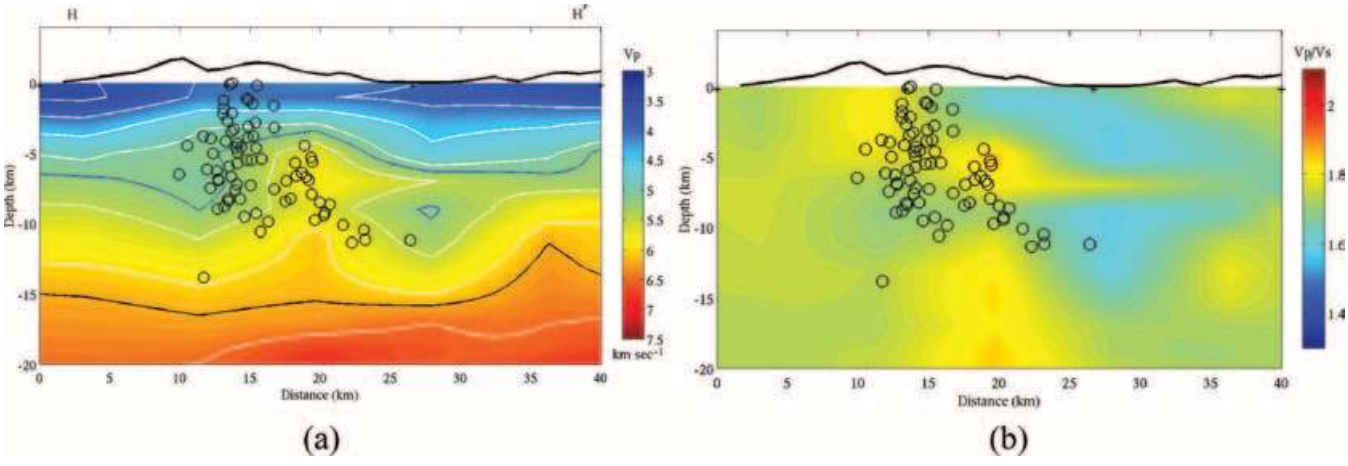

Figure 17. Vertical slices of (a) the *P*-wave velocity model and (b) the V_P/V_S ratio model with seismicity along cross-section H–H′ (Fig. 12) across the Tatun-Chilung volcano group in northern Taiwan. A region of low V_P and high V_P/V_S ratio has been imaged beneath the high volcano that may suggest potential for the partial melting or a magma reservoir.

subsurface structures observed in our 3-D velocity models. In general, Bouguer gravity anomalies increase gradually from west to east across the high mountains with a higher gradient in the east than in the west. The higher gradient in eastern Taiwan may be interpreted as the result of a rapid change of crust structure and density at depth, particularly the Moho depth. Several cross-sectional views of 3-D velocity models (Fig. 11) reveal a gradual thickening of the crust from west to east until it reaches its maximum value beneath the eastern Central Mountain Range. The Moho depth decreases sharply toward the east and merges with the crust of the Philippine Sea Plate. Thus, our 3-D velocity models successfully explain most of the observed gravity anomalies in the Taiwan region.

CONCLUSIONS

Modern high-resolution earthquake data collected by the Central Weather Bureau in the Taiwan region has provided an unprecedented opportunity to allow us to resolve 3-D crust and upper mantle

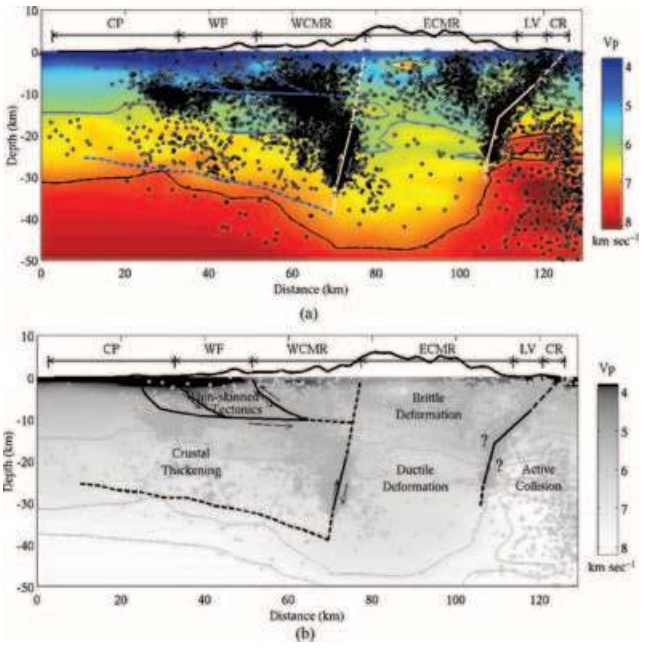

Figure 18. (a) *P*-wave velocity profile and relocated seismicity along cross-section I–I′ in central Taiwan (Fig. 12) and (b) a preliminary tectonic interpretation for central Taiwan. The crust thickened and uplifted beneath the Central Mountain Range. The eastern Central Mountain Range is bounded apparently by two westward steeply dipping boundary faults, inside which the thickened crust is characterized by a high-velocity, high-seismicity brittle upper crust and by a low-velocity, aseismic and ductile mid to lower crust. The eastern boundary fault clearly separates the oceanic crust to the east and the continental crust to the west. The western boundary fault was activated only after the 1999 Chi-Chi earthquake sequence, where fault movement determined by Chen *et al.* (2002) is presented. Thin-skinned tectonics may explain satisfactorily the deformation of the upper crust beneath western central Taiwan whereas the eastern Central Mountain Range behaves as a backstop. Scattered lower crust seismicity beneath western Taiwan may represent deformation associated with the tectonic process of crust thickening and plate convergence. CP, Coastal Plain; WF, Western Foothills; WCMR, western Central Mountain Range (Hsueshan Range); ECMR, eastern Central Mountain Range; LV, Longitudinal Valley; CR, Coastal Range.

structural models pertinent to the collision and subduction processes in the area. The collision zone can be best described near the Taitung area in southeastern Taiwan by the steeply eastward dipping active fault zone extending to ∼30 km depth along a highly fractured region associated with the initial phase of plate collision, and near the Hualien area of central eastern Taiwan by the steeply westward dipping active fault zone extending from near the surface to ∼30 km depth along an advanced collision plate boundary separating continental and oceanic crust. Behind the collision, the uplifted north–south trending Central Mountain Range and its corresponding mirror images of the Moho depth variations manifest the deformation of the Eurasian Plate from the collision process.

The depth to the Moho varies significantly beneath Taiwan, especially along the east–west direction perpendicular to the north–south trending tectonic boundaries. The Moho depth is ∼35 km beneath the Western Foothills, deepens to ∼50–55 km beneath the eastern Central Mountain Range, decreases quickly across the collision boundary beneath the Longitudinal Valley and Coastal Range, and merges offshore into the thin Philippine Sea Plate. The Central Mountain Range is bounded in central Taiwan by two steeply westward dipping active faults extending from the surface to ∼30 km depth. Between the two boundary faults, it is characterized by a ∼15 km brittle, high-velocity and seismically active upper crust, and by the ductile, low-velocity and aseismic mid to lower crust. High temperature and high geothermal activity due to excess heat supplied from the oceanic upper mantle beneath the thin Philippine Sea Plate and the surrounding hot upper mantle beneath the Eurasian Plate as well as the potential of shear heating from active collision may contribute to the thickening and uplift of continental crust beneath the Central Mountain Range.

No apparent seismicity can be found within the sedimentary basins all over the Taiwan region, which is very reasonable since the loosely coupled sediments in many young basins are not strong enough to sustain the accumulation of regional strains to release instantly as an earthquake. However, a few basins are either bounded on one side by an active fault, e.g. the Dorfun-Pin Fault to the east of the Hsin-Chu Basin, the Chao-Chou Fault to the east of the Pintung Basin, or are characterized by potential blind faults, e.g. the Taichung Basin, the Chia-Yi-Tainan Basin and the Ilan Basin.

The subduction zone geometry in northeastern Taiwan can be clearly imaged by the high-velocity region and delineated by the linearly distributed deep seismicity. Concentrated seismicity in the overriding Eurasian Plate reveals the significance of deformation in northern and southern Taiwan associated with the subduction process. Behind the subduction, a region of low V_P but high V_P/V_S ratio characterizes the Tatun-Chilung volcanic group in northern Taiwan, which may indicate a potential magma reservoir at 5 to 10 km depth. Two steeply dipping areas of linear seismicity beneath the Tatun volcano group may mark the upward paths of deep magmatic materials.

ACKNOWLEDGMENTS

We thank Dr Harley M. Benz of the US Geological Survey for allowing us to use his 3-D tomographic inversion software in this and related studies. We also thank CWB for providing arrival time data from their island-wide seismic network. Critical reviews and comments by Drs Thorsten Becker, Chengsung Wang and Serge E. Lellemand are highly appreciated. This study was sponsored by the State of Tennessee Centers of Excellence Program. The preliminary draft of this paper was completed during a sabbatical visit of one of the authors (JMC) to the Institute of Earth Sciences, Academia Sinica, Taipei, Taiwan, sponsored by the Professional Development Program of the College of Arts and Sciences, the University of Memphis, and by the Visiting Professor Program of the National Research Council, Taiwan (NSC 93-2811-M-001-012). This is CERI contribution number 487.

REFERENCES

Angelier, J., Chu, H.-T. & Lee, J.-C., 1997. Shear concentration in a collision zone: kinematics of the Chihshang Fault as revealed by outcrop-scale quantification of active faulting, Longitudinal Valley, eastern Taiwan, *Tectonophysics,* **274**(1–3), 117–143.

Benz, H.M., Chouet, B.A., Dawson, P.B., Lahr, J.C., Page, R.A. & Hole, J.A., 1996. Three-dimensional P and S wave velocity structure of Redoubt Volcano, Alaska, *J. geophys. Res.,* **101**(4), 8111–8128.

Chen, C.-S., Chen, C.-C. & Chou, K., 1998. Deep electrical structure of Taiwan as inferred from magnetotelluric observations, *Terres. Atmos. Ocean. Sci.,* **9**(1), 51–68.

Chen, H., Chiu, J.-M., Pujol, J., Kim, K.-H., Chen, K.-C., Huang, B.-S., Yeh, Y.-H. & Chiu, S.-C., 2005. A simple algorithm for local earthquake location using 3-dimensional Vp and Vs Models—test examples in the central USA and Taiwan regions, *Bull. seism. Soc. Am.* (in review).

Chen, K.-C., 1995a. Earthquake studies using the PANDA and PANDAII seismic array, *PhD thesis*, CERI/Department of Geological Science, The University of Memphis, Memphis, TN.

Chen, K.-C., Huang, B.-S., Wang, J.-H. & Yen, H.-Y., 2002. Conjugate thrust faulting associated with the 1999 Chi-Chi, Taiwan, earthquake sequence, *Geophys. Res. Lett.,* **29**(8), doi:10.1029/2001GL014250.

Chen, K.-P., 1998. Study of shallow structure beneath Kaoshiung–Pingtung region using local earthquake data, *PhD thesis*, Institute of Geophysics, National Central University, Jungli, Taiwan.

Chen, Y.L., 1995b. Three-dimensional velocity structure and kinematic analysis in the Taiwan area, *PhD thesis*, National Central University, Jungli, Taiwan.

Chiu, J.M., Chen, H., Pujol, J., Chiu, S.C. & Withers, M., 2003. A new earthquake catalog for the new Madrid seismic zone using a preliminary 3-dimensional Vp and Vs velocity model, *Seism. Res. Lett.,* **74**(1), 69.

Eberhart-Phillips, D., 1986. Three-dimensional velocity structure in Northern California Coast Ranges from inversion of local earthquake arrival times, *Bull. seism. Soc. Am.,* **76**(4), 1025–1052.

Ho, C.S., 1999. *An Introduction to the Geology of Taiwan. Explanatory Text of the Geologic Map of Taiwan,* Central Geological Survey/The Ministry of Economic Affairs, Taiwan.

Hole, J.A., Brocher, T.M., Klemperer, S.L., Parsons, T.E., Benz, H.M. & Furlong, K.P., 2000. Three-dimensional seismic velocity structure of the San Francisco Bay area, *J. geophys. Res.,* **105**(6), 13 859–13 874.

Hu, J.-C., Angelier, J., Yu, S.-B., Lallemand, S.E. & Tsien, H.-H., 1997. An interpretation of the active deformation of southern Taiwan based on numerical simulation and GPS studies, *Tectonophysics,* **274,** 145–169.

Huang, B.-S., 1998. Array observations of PKP phases across Taiwan region: a test on regional tomographic models, *EOS, Trans. Am. geophys. Un.,* **79**(24), W79.

Hwang, W.-T. & Wang, C.-Y., 1993. Sequential thrusting model for mountain building; constraints from geology and heat flow of Taiwan, *J. geophys. Res.,* **98**(6), 9963–9973.

Kim, K.-H., 2003. Subsurface structure, seismicity patterns, and their implication to tectonic evolution in Taiwan, *PhD thesis*, University of Memphis, Memphis, TN.

Kim, K.H., Chiu, J.M., Pujol, J., Chen, K.C. & Ma, K.F., 2005a, Active collision plate boundary beneath the Hualien area in the central eastern Taiwan (in review), *Geophys. Res. Lett.*

Kim, K.H., Chiu, J.M., Pujol, J. & Chen, K.C., 2005b. Active plate collision zone in eastern Taiwan: a seismogenic view from 3-D velocity images and relocated hypocenters (in review), *Bull. seism. Soc. Am.*

Kim, K.W., Chang, G., Ma, K.F., Chiu, J.M. & Chen, K.C., 2005c. Modern seismic observations in the Tatun volcano region of northern Taiwan: seismic/volcanic hazard adjacent to the Taipei metropolitan area (in review), *TAO*.

Kissling, E., 1988. Geotomography with local earthquake data, *Rev. Geophys.,* **26**(4), 659–698.

Lees, J.M. & Crosson, R.S., 1989. Tomographic inversion for three-dimensional velocity structure at Mount St. Helens using earthquake data, *J. geophys. Res.,* **94**(5), 5716–5728.

Liang, W.T. & Chiu, J.M., 2005. Anomalous Pn waves observed in eastern Taiwan: implications of an elevated upper mantle beneath the active collision suture zone (in review), *Geophys. Res. Lett.*

Lin, C.-H., 2000. Thermal modeling of continental subduction and exhumation constrained by heat flow and seismicity in Taiwan, *Tectonophysics,* **324**(3), 189–201.

Liu, C.-C., Yu, S.-B. & Angelier, J., 1990. Vertical crustal movements in eastern Taiwan and their tectonic implications, *Tectonophysics,* **183**(1–4), 111–119.

Ma, K.-F., Wang, J.-H. & Zhao, D., 1996. Three-dimensional seismic velocity structure of the crust and uppermost mantle beneath Taiwan, *J. Phys. Earth,* **44**(2), 85–105.

Okubo, P.G., Benz, H.M. & Chouet, B.A., 1997. Imaging the crustal magma sources beneath Mauna Loa and Kilauea volcanoes, Hawaii, *Geology,* **25**(10), 867–870.

Paige, C.C. & Saunders, M.A., 1982. LSQR: an algorithm for sparse linear equations and sparse least squares, *ACM Trans. Math. Software,* **8,** 43–71.

Pavlis, G.L. & Booker, J.R., 1980. The mixed discrete-continuous inverse problem; application to the simultaneous determination of earthquake hypocenters and velocity structure, *J. geophys. Res.,* **85**(9), 4801–4810.

Podvin, P. & Lecomte, I., 1991. Finite difference computation of traveltimes in very contrasted velocity models; a massively parallel approach and its associated tools, *Geophys. J. Int.,* **105**(1), 271–284.

Pujol, J., 1995. Application of the JHD technique to the Loma Prieta, California, mainshock–aftershock sequence and implications for earthquake location, *Bull. seism. Soc. Am.,* **85**(1), 129–150.

Pujol, J., 2000. Joint event location - the JHD technique and applications to data from local seismic networks, in *Advances in Seismic Event Location,* pp. 163–204, eds Thurber, C.H. & Rabinowitz, N., Kluwer Academic Publishers, Dordrecht.

Pujol, J. et al, 1989. 3-D P- and S-wave velocity structure of the Andean Foreland in San Juan, Argentina, from local earthquakes, in *AGU Fall Meeting, San Francisco,* EOS, **70**(43), pp. 1361.

Rau, R.-J. & Wu, F.T., 1995. Tomographic imaging of lithospheric structures under Taiwan, *Earth planet. Lett.,* **133,** 517–532.

Roecker, S.W., 1993. Tomography in zones of collision; practical considerations and examples, in *Seismic Tomography: Theory and practice,* pp. 584–612, eds Iyer, H.M. & Hirahara, K., Chapman and Hall, London.

Roecker, S.W., Yeh, Y.H. & Tsai, Y.B., 1987. Three-dimensional P and S wave velocity structures beneath Taiwan; deep structure beneath an arc-continent collision, *J. geophys. Res.,* **92**(10), 10 547–10 570.

Shen, P., 1999. Simultaneous traveltime inversion for 3D velocity model and earthquake locations: application to the Northridge, California, 1994 mainshock-aftershock sequence, *MS thesis*, Geological Sciences, The University of Memphis, Memphis, TN (unpublished).

Shih, R.C. et al, 1998. Preliminary crustal structures across central Taiwan from modeling of the onshore-offshore wide-angle seismic data, *Terres. Atmos. Ocean. Sci.,* **9**(3), 317–328.

Snoke, A.J. & Lahr, J.C., 2001. Locating earthquakes: at what distances can the Earth no longer be treated as flat?, *Seism. Res. Lett.,* **72**(5), 538–541.

Suppe, J., 1984. Kinematics of arc–continent collision, flipping of subduction, and back-arc spreading near Taiwan, *Mem. Geol. Soc. China,* **6,** 21–33.

Suppe, J., 1987. The active Taiwan mountain belt, in *Anatomy of Mountain Chains,* pp. 277–293, eds Shaer, J.P. & Rodgers, J., Princeton University Press, Princeton, NJ.

Tsai, Y.-B., 1986. Seismotectonics of Taiwan, *Tectonophysics,* **125,** 17–37.

Villasenor, A., Scarpa, R., Patane, G., Vinciguerra, S., Benz, H.M., Filippi, L. & De Luca, G., 1998. Three-dimensional P-wave velocity structure of Mt. Etna, Italy, *Geophys. Res. Lett.,* **25**(11), 1975–1978.

Wang, C.-Y. & Shin, T.-C., 1998. Illustrating 100 years of Taiwan seismicity, *Terres. Atmos. Ocean. Sci.,* **9**(4), 589–614.

Wang, J.-H., Chen, K.-C. & Lee, T.-Q., 1994. Depth distribution of shallow earthquakes in Taiwan, *J. Geol. Soc. China,* **37**(2), 125–142.

Yeh, Y.H. et al, 1998. Onshore/offshore wide-angle deep seismic profiling in Taiwan, *Terres. Atmos. Ocean. Sci.,* **9**(3), 301–316.

Yen, H.-Y., Tsai, Y.-B., Yeh, Y.-H., Lin, C.-H. & Chen, K.-J., 1995. Gravity survey of Taiwan, *J. Phys. Earth,* **43**(6), 685–696.

Yen, H.-Y., Yeh, Y.-H. & Wu, F.T., 1998. Two-dimensional crustal structures of Taiwan from gravity data, *Tectonics,* **17**(1), 104–111.

Yu, S.-B. & Liu, C.-C., 1989. Fault creep on the central segment of the Longitudinal Valley Fault, eastern Taiwan, *Proc. Geol. Soc. China,* **32**(3), 209–231.

Yu, S.-B., Chen, H.-Y., Kuo, L.-C., Lallemand, S.E. & Tsien, H.-H., 1997. Velocity field of GPS stations in the Taiwan area, *Tectonophysics,* **274**(1–3), 41–59.

Zhao, D., Hasegawa, A. & Horiuchi, S., 1992. Tomographic imaging of P and S wave velocity structure beneath northeastern Japan, *J. geophys. Res.,* **97**(13), 19 909–19 928.